

 Open access • Posted Content • DOI:10.1101/175091

## The roles of Conserved Domains in DEMETER-Mediated Active DNA Demethylation in *planta* — [Source link](#)

Chi Zhang, Yu-Hung Hung, Xiang-Qian Zhang, Dapeng Zhang ...+5 more authors

**Institutions:** North Carolina State University, South China Agricultural University, Saint Louis University, National Institutes of Health ...+1 more institutions

**Published on:** 10 Aug 2017 - bioRxiv (bioRxiv)

**Topics:** DNA demethylation, DNA methylation, Genomic imprinting and Processivity

Related papers:

- [Control of DEMETER DNA demethylase gene transcription in male and female gamete companion cells in \*Arabidopsis thaliana\*](#)
- [Epigenetic role for the conserved Fe-S cluster biogenesis protein AtDRE2 in \*Arabidopsis thaliana\*](#)
- [Overproduction of stomatal lineage cells in \*Arabidopsis\* mutants defective in active DNA demethylation](#)
- [Regulation of Active DNA Demethylation by an  \$\alpha\$ -Crystallin Domain Protein in \*Arabidopsis\*](#)
- [The DNA demethylase ROS1 targets genomic regions with distinct chromatin modifications.](#)

Share this paper:    

View more about this paper here: <https://typeset.io/papers/the-roles-of-conserved-domains-in-demeter-mediated-active-4g8k3p52m7>

1 Title: The roles of Conserved Domains in DEMETER-Mediated Active DNA Demethylation in  
2 *planta*

3

4 Changqing Zhang<sup>1,2,\*</sup>, Yu-Hung Hung<sup>1,2,\*</sup>, Xiang-Qian Zhang<sup>1,2,3,\*</sup>, Dapeng Zhang<sup>4,5</sup>, Wenyan  
5 Xiao<sup>4</sup>, Lakshminarayan M. Iyer<sup>6</sup>, L. Aravind<sup>6</sup>, Jin Hoe Huh<sup>7</sup> and Tzung-Fu Hsieh<sup>1,2,\*</sup>

6 Affiliations:

7 <sup>1</sup>Department of Plant and Microbial Biology, North Carolina State University, Raleigh, NC  
8 27695, USA

9 <sup>2</sup>Plants for Human Health Institute, North Carolina State University, North Carolina Research  
10 Campus, Kannapolis, NC 28081, USA

11 <sup>3</sup>Guangdong Engineering Research Center of Grassland Science, College of Forestry and  
12 Landscape Architecture, South China Agricultural University, Guangzhou 510642, China.

13 <sup>4</sup>Department of Biology, St. Louis University, St. Louis, MO 63103, USA

14 <sup>5</sup>Program of Bioinformatics and Computational Biology, St. Louis University, St. Louis, MO  
15 63103, USA

16 <sup>6</sup>National Center for Biotechnology Information, National Library of Medicine, National  
17 Institutes of Health, Bethesda, MD 20894, USA

18 <sup>7</sup>Department of Plant Science, Plant Genomics and Breeding Institute, and Research Institute of  
19 Agriculture and Life Sciences, Seoul National University, Seoul 08826, Republic of Korea

20 \*These authors contribute equally to this study.

21 Correspondence and requests for materials should be addressed to T.-F.H. [thsieh3@ncsu.edu](mailto:thsieh3@ncsu.edu)

22 **Abstract**

23 DNA methylation plays critical roles in maintaining genome stability, genomic imprinting,  
24 transposon silencing, and development. In Arabidopsis genomic imprinting is established in the  
25 central cell by DEMETER (DME)-mediated active DNA demethylation, and is essential for seed  
26 viability. DME is a large polypeptide with multiple poorly characterized conserved domains.  
27 Here we show that the C-terminal enzymatic core of DME is sufficient to complement *dme*  
28 associated developmental defects. When targeted by a native DME promoter, nuclear-localized  
29 DME C-terminal region rescues *dme* seed abortion and pollen germination defects, and  
30 ameliorates CG hypermethylation phenotype in *dme-2* endosperm. Furthermore, targeted  
31 expression of the DME N-terminal region in wild-type central cell induces *dme*-like seed  
32 abortion phenotype. Our results support a bipartite organization for DME protein, and suggest  
33 that the N-terminal region might have regulatory function such as assisting in DNA binding and  
34 enhancing the processivity of active DNA demethylation in heterochromatin targets.

35

36

37 Double fertilization during sexual reproduction in flowering-plants is a unique process that  
38 underlies the distinctive epigenetic reprogramming of plant gene imprinting. In the ovule, a  
39 haploid megaspore undergoes three rounds of mitoses to produce a 7-celled, 8 nuclei embryo sac  
40 that consists of egg, central, and accessory cells<sup>1</sup>. During fertilization pollen grain elongates and  
41 delivers two sperm nuclei to the female gametophyte to fertilize the egg cell and the central cell,  
42 respectively. The fertilized egg cell forms the embryo that marks the beginning of the subsequent  
43 generation. Fertilization of the central cell initiates the development of endosperm that  
44 accumulates starch, lipids, and storage proteins and serves as a nutrient reservoir for the  
45 developing embryo<sup>2,3</sup>. Endosperm is the major tissue where gene imprinting takes place in plant.  
46 Genomic imprinting is the differential expression of the two parental alleles of a gene depending  
47 on their parent-of-origin, and is an example of inheritance of differential epigenetic states. In  
48 Arabidopsis, MET1-mediated DNA methylation and DME demethylation are two modes of  
49 epigenetic regulation critical for imprinted expression of many genes<sup>4, 5, 6, 7, 8</sup>. For example,  
50 DEMETER (DME) is required for the expression of *MEA*, *FIS2*, and *FWA* in the central cell and  
51 in the endosperm while MET1 is responsible for the silencing of *FIS2* and *FWA* paternal alleles<sup>4</sup>,  
52<sup>7</sup>. Gene imprinting is essential for reproduction in Arabidopsis, and seeds that inherit a maternal  
53 *dme* allele abort due to failure to activate *MEA* and *FIS2*, essential components of the endosperm  
54 PRC2 complex required for seed viability, in the central cell<sup>4,9</sup>.

55 *DME* encodes a bifunctional 5mC DNA glycosylase/lyase required for active DNA  
56 demethylation in the central cell and the establishment of endosperm gene imprinting in  
57 Arabidopsis<sup>5</sup>. Additionally, paralogs of DME, REPRESSOR OF SILENCING 1 (ROS1), DML2,  
58 and DML3 are required to counteract the spread of DNA methylation mediated by the RNA-  
59 directed DNA methylation (RdDM) machinery into nearby coding genes<sup>10,11</sup>. The three regions

60 in the C-terminal half of DME protein (the A, Glycosylase, and the B regions, or as the AGB  
61 region hereafter) are conserved among the DME/ROS1 DNA glycosylase clade, and are required  
62 for DME 5mC excision activity *in vitro*. Thus, the AGB region comprise the minimal catalytic  
63 core for the enzymatic function, catalyzing direct excision of 5mC from DNA and initiating  
64 active DNA demethylation that influences transcription of nearby genes <sup>5, 9, 12</sup>.

65 In Arabidopsis, DME-mediated DNA demethylation is preferentially targeted to small,  
66 AT-rich, and nucleosome-poor euchromatic transposons that flank coding genes <sup>13</sup>. Consequently,  
67 demethylation in the central cell influences expression of adjacent genes only in the maternal  
68 genome, and is a primary mechanism of gene imprinting in plant <sup>5, 13, 14, 15</sup>. In addition to small  
69 TEs near coding sequences, DME also targets gene-poor heterochromatin regions for  
70 demethylation <sup>13</sup>. The mechanism of DME recruitment to its target sites is not known. Studies in  
71 ROS1 have uncovered several players required in the ROS1 demethylation pathway <sup>16, 17, 18</sup>.  
72 Among them *IDM1* encodes a novel histone acetylase that preferentially acetylates H3K18 and  
73 H3K23 *in vitro*, and ROS1 target loci are enriched for H3K18 and K23 acetylation *in vivo* in an  
74 IDM1-dependent manner <sup>19</sup>. Thus, IDM1 marks ROS1 target sites by acetylating histone H3 to  
75 create a permissible chromatin environment for ROS1 function. The Arabidopsis SSRP1  
76 (STRUCTURE SPECIFIC RECOGNITION PROTEIN1), a component of the FACT (facilitates  
77 chromatin transcription/transaction) histone chaperone complex, has been shown to regulate  
78 DNA demethylation and gene imprinting in Arabidopsis <sup>20</sup>. Linker histone H1 functions in  
79 chromatin folding and gene regulation <sup>21, 22, 23, 24</sup>, and was shown to interact with DME in a yeast  
80 two-hybrid screen and in an *in vitro* pull-down assay <sup>25</sup>. Loss-of-function mutations in *H1* genes  
81 affect the imprinted expression of *MEA* and *FWA* in Arabidopsis endosperm, and impair  
82 demethylation of their maternal alleles, suggesting that H1 might participate in the DME

83 demethylation process by interaction with DME<sup>25</sup>.

84 Computational analysis showed that the DME/ROS1 like DNA glycosylases contain a  
85 core with multiple conserved globular domains, and except for the well-characterized  
86 glycosylase domain, very little is known about the function of the other domains. Here we show  
87 that the C-terminal region of DME necessary for 5-methylcytosine excision activity *in vitro* is  
88 sufficient to complement *dme* seed abortion and pollen germination defect, and partially rescue  
89 DNA hypermethylation phenotype in endosperm. We present evidence that the region N-  
90 terminal to the glycosylase domain can affect endogenous DME activity in a dominant negative  
91 manner when ectopically expressed in the nuclei of wild-type central cells. We propose a  
92 bipartite structural and functional organization model for the DME/ROS1 family of DNA  
93 glycosylases consisting the modular C-terminal AGB region that can substitute for DME's  
94 developmental function and the NTD region that might have regulatory functions such as  
95 assisting DNA binding and enhancing the processivity of demethylation in heavily methylated  
96 genomic regions.

97

## 98 **Results**

99 **The DME catalytic core region is sufficient to complement *dme* associated developmental**  
100 **defects.** Previous studies have revealed that the C-terminal half of DME comprising the three  
101 conserved A, Glycosylase, and B regions (the AGB region, as shown in Supplementary Fig. 1a)  
102 are required for *in vitro* 5mC excision activity<sup>5</sup>, and deletion of the non-conserved linker  
103 between domain A and the glycosylase domain (interdomain 1; ID1) does not affect DME *in*  
104 *vitro* enzymatic activity<sup>26,27</sup>. Thus, the AGB region is thought to be the core catalytic region for  
105 DME *in vitro* enzymatic activity. However, it is unknown whether the AGB region alone is

106 sufficient for DME function *in vivo*. To determine if the AGB region is functional *in vivo*, we  
107 tested if expressing the AGB region in the central cell can complement *dme* seed abortion  
108 phenotype. A transgene carrying a 3.1-kb *DME* cDNA that encodes the C-terminal half of DME  
109 ( $DME^{CTD}$ , residue 936-1987) under the control of a native DME promoter was introduced into  
110 *DME/dme-2* heterozygous plants by using the floral dipping method<sup>28</sup>. Since  $DME^{CTD}$  lacks a  
111 nuclear localization signal (data not shown), a classical SV40 nuclear localization signal  
112 (PKKKPKV) was introduced in front of the C-terminal fragment (designated as  $nDME^{CTD}$ , see  
113 Supplementary Fig. 1b) to ensure proper nuclear localization. We obtained multiple independent  
114 transgenic lines and assessed the transgene's ability to complement *dme-2* seed abortion  
115 phenotype.

116 The self-pollinated *DME/dme-2* plants produce 50% of normal seed that inherited wild type  
117 DME maternal allele, and the other 50% of aborted seed that inherited mutant *dme-2* maternal  
118 allele. In self-pollinated transgenic plants that carry a single locus of  $nDME^{CTD}$  or  $DME^{FL}$  (full  
119 length DME.2 cDNA, major isoform of DME<sup>29</sup>) transgenes, we observed about 25% aborted  
120 seeds among independent transgenic lines, indicating that  $nDME^{CTD}$  and  $DME^{FL}$  complement  
121 *dme* seed abortion phenotype (Fig. 1a, b, Supplementary Table 1). In addition, we also  
122 transformed  $nDME^{CTD}$  and  $DME^{FL}$  into *dme-2/dme-2* homozygous plants (see Materials and  
123 Methods for isolation and characterization of *dme-2/dme-2* homozygous lines in *Col-gl*), both  
124 constructs produced T1 transgenic plants that displayed expected 50% seed abortion rate (Fig. 1b,  
125 Supplementary Table 1). Seed abortion caused by *dme* mutations is in part due to defects in  
126 activating imprinted PRC2 subunit genes required for endosperm development<sup>5, 9, 30, 31, 32</sup>. We  
127 use qRT-PCR to check if  $nDME^{CTD}$  also restores DME target genes expression in the central cell.  
128 Indeed, *FIS2* and *FWA* expression is restored in the complemented lines (Fig. 1c). Thus

129 nDME<sup>CTD</sup> can substitute for the endogenous DME activity for seed viability, and active DME  
130 target genes expression.

131 In addition to maternal effects on seed viability<sup>9</sup>, mutations in DME also affect pollen  
132 function in Col-0. When *DME/dme-2* heterozygous plants are self-pollinated, only about 20-30%  
133 of the viable F1 progeny are heterozygous (Supplementary Table 2), due to decreased *dme* pollen  
134 germination rate<sup>33</sup>. To test whether nDME<sup>CTD</sup> can rescue *dme* pollen phenotype, we pollinated  
135 wild type Col-0 with pollen derived from transgenic lines that are homozygous for the *dme-2*  
136 allele and carry a single locus of the nDME<sup>CTD</sup> transgene (*dme-2/dme-2; nDME<sup>CTD</sup>/~*). If  
137 nDME<sup>CTD</sup> does not complement *dme-2* pollen germination defects, we expect roughly half of the  
138 F1 progeny will carry the nDME<sup>CTD</sup> transgene (hygromycin resistant) because mutant pollen  
139 with or without the transgene would germinate with equal frequency. Instead, we observed 65% -  
140 90% of the F1 progeny are hygromycin resistant (Table 1), indicating that nDME<sup>CTD</sup>  
141 complements *dme-2* pollen germination defect. These results show that expressing the C-  
142 terminal half of DME protein in the nucleus is sufficient to rescue *dme* visible phenotypes *in*  
143 *planta*.

144  
145 **nDME<sup>CTD</sup> partially rescue *dme-2* CG hypermethylation phenotype in the endosperm.** In  
146 Arabidopsis seed viability depends on the DME activity in the central cell to activate the  
147 MEDEA/FIS2/MSI1/FIE PRC2 complex required for endosperm development. In addition,  
148 DME is required to demethylate multiple maternally (*MEGs*) or paternally expressed imprinted  
149 genes (*PEGs*) to establish their parent-of-origin specific expression patterns in the endosperm<sup>13</sup>,  
150<sup>15</sup>. Thus, in *dme* mutant endosperm, discrete genomic loci targeted by DME for demethylation  
151 are hypermethylated<sup>13</sup>. Since nDME<sup>CTD</sup> complements *dme* seed abortion, and activates DME



152 target gene expression (Fig. 1), we assumed it does so by demethylating the central cell genome  
153 and activating PRC2 genes essential for seed development. To test this hypothesis, and to  
154 examine the extend of nDME<sup>CTD</sup> demethylation activity *in vivo*, we manually isolated *nDME<sup>CTD</sup>*-  
155 complemented endosperm (*dme-2/dme-2;nDME<sup>CTD</sup>/nDME<sup>CTD</sup>*), determined the DNA  
156 methylation profile by whole genome bisulfite sequencing, and compared the complemented  
157 methylomes to those of wild-type and *dme-2* endosperm. Methylomes from three independent  
158 lines were generated and compared with that of *dme-2* endosperm. We observed although the  
159 differentially methylated regions (DMRs) between each independent lines do not completely  
160 overlap, the DMRs unique to each line are also demethylated in other lines (Supplementary Fig.  
161 2, 3), suggesting that the number of overlapped DMRs was underestimated due to the cutoff used  
162 in defining the DMRs, similar to what's observed in a recent study<sup>34</sup>. We therefore used the  
163 combined reads from three independent lines for the subsequent analyses so that all comparisons  
164 are confined to the same cutoff criteria (see Materials and Methods). As expected, several DME  
165 regulated *MEGs* and *PEGs* are demethylated compared to *dme-2* endosperm, indicating that  
166 nDME<sup>CTD</sup> is correctly recruited to these loci for demethylation (Fig. 2a). We focused our analysis  
167 on previously determined differentially methylated sites between *dme-2* and wild-type  
168 endosperm (*dme* hyper-DMRs, the DME canonical targets)<sup>13, 15</sup>. Overall, the CG methylation  
169 levels in these canonical DME target sites are reduced in the complemented endosperm,  
170 indicating that nDME<sup>CTD</sup> is directed to these endogenous DME target sites for demethylation.  
171 However, compared to wt endosperm, these *dme* hyper-DMRs are demethylated to a lesser  
172 degree by the nDME<sup>CTD</sup> (Fig. 2b). Thus nDME<sup>CTD</sup> only partially rescues the *dme* CG  
173 hypermethylation phenotype in the endosperm. The DMRs of *dme* relative to wild-type  
174 endosperm or to *nDME<sup>CTD</sup>*-complemented endosperm partially overlap (Supplemental Fig. 4).

175 However, among the DMRs unique to  $nDME^{CTD}$ , we also observed decreased CG methylation in  
176 WT endosperm compared to *dme*, indicating that they are also demethylated by the endogenous  
177 DME. Similarly, among the DMRs unique to wt endosperm, these regions are also demethylated  
178 by the  $nDME^{CTD}$ . Thus  $nDME^{CTD}$  appears to partially demethylate the majority of the loci  
179 targeted by the endogenous DME. These observations also suggest that intact full-length DME  
180 protein is required for robust and complete demethylation *in vivo*.

181 We next examined the methylome of *dme-2* endosperm complemented by the full length  
182 *DME.2* cDNA (designated as  $DME^{FL}$ ). Unexpectedly, based on the number of DMRs between  
183 *dme* and  $DME^{FL}$ -complemented endosperm and the level of CG methylation within the DMRs  
184 (Fig. 2c),  $DME^{FL}$  appears to be less active compared to endogenous DME, or to  $nDME^{CTD}$ , albeit  
185 it being able to complement *dme* seed abortion (Fig. 1b)<sup>9, 35</sup>. Since the  $DME^{FL}$  transgene only  
186 differs from  $nDME^{CTD}$  by the N-terminal region, reduced activity of  $DME^{FL}$  compared to  
187  $DME^{CTD}$  cannot be attributed to the lack of introns or 3' flanking sequences that might be needed  
188 for robust DME protein production. Indeed, we found both transgenes are expressed at  
189 comparable levels in  $DME^{FL}$ - and  $nDME^{CTD}$ -complemented lines used in the methylome study  
190 (Supplemental Fig. 5), indicating lower activity of  $DME^{FL}$  compared to  $nDME^{CTD}$  is not due to  
191 their differential transcript abundance. Nevertheless, comparison of CG methylation levels in  
192 DMR regions unique to  $DME^{FL}$ ,  $nDME^{CTD}$ , or endogenous DME also reveals that unique DMR  
193 regions are more or less hypomethylated in WT or in complemented endosperm relative to *dme*  
194 endosperm. Thus the methylome difference between wt,  $DME^{FL}$ -, and  $nDME^{CTD}$ -complemented  
195 endosperm appears to be more in the degree of demethylation, rather than in targeting specificity.  
196

197 **Function of the N-terminal region in DME-mediated active DNA demethylation.** The *dme-2*  
198 allele is caused by an activation-tagging T-DNA insertion in the middle of the A region  
199 (Supplementary Fig. 1a)<sup>9</sup>. We found that in floral buds of *dme-2/dme-2* plants, the endogenous  
200 *DME* transcripts downstream of T-DNA insertion site is greatly reduced compared to wild-type  
201 Col-0 plants, but the level of *DME* transcripts upstream of the T-DNA insertion site is relatively  
202 high (Supplementary Fig. 6). We suspected these transcripts could produce truncated form of  
203 *DME* proteins that might interfere with the *DME*<sup>FL</sup> transgene activity. To test this hypothesis, we  
204 transformed wild-type Col-0 plants with an engineered GFP-tagged *DME* NTD (using the  
205 genomic DNA sequence upstream of T-DNA insertion site, encoding residues 1-1022, designated  
206 as *DME*<sup>NTD</sup>-*GFP*) transgene mimicking the *dme-2* T-DNA insertion (Supplementary Fig. 1B).  
207 Clear GFP signals are observed in the central cell nuclei of transgenic lines (data not shown). We  
208 also observed about one third of transgenic lines showing apparent *dme-2* like seed abortion  
209 phenotype, with abortion rates ranging from 10% to ~ 40% (Supplementary Table 3, 4) in the T1  
210 plants, suggesting that expression of *DME*<sup>NTD</sup> has a dominant negative effect on endogenous  
211 *DME* protein.

212 To minimize the possibility and the degree of transgene induced sense co-suppression, we  
213 reverse translated *DME*<sup>NTD</sup> protein sequence into cDNA sequence using the human codon usage  
214 table. As a result, the re-engineered “humanized” version of NTD (*mDME*<sup>NTD</sup>) codes for the  
215 identical protein sequence but with no significant nucleotide sequence similarity to the original  
216 cDNA sequence to induce co-suppression (Supplementary Table 5). In addition, a GFP tag was  
217 added to the C-terminus (*mDME*<sup>NTD</sup>-*GFP*) to monitor its expression (Fig. 3a). We generated 28  
218 independent transgenic lines, and among them 16 lines showed seed abortion rate of 5% - 52%  
219 (Supplementary Table 3, 6). The aborted seeds resemble *dme* mutant seeds with abnormal

220 endosperm, arrested embryo, and shriveled brown seeds (Fig. 3b, c). We selected four lines with  
221 high, medium, or no seed abortion rate (Fig. 3d), and assessed the endogenous DME transcript  
222 abundance. As shown in Fig. 3e, among lines with different seed abortion rate, the endogenous  
223 DME mRNA abundance is similar to that of the vector control line, indicating the severity of  
224 seed abortion phenotype is not due to interference of endogenous *DME* transcripts. Furthermore,  
225 the rate of seed abortion is positively correlated with the levels of *mDME<sup>NTD</sup>-GFP* mRNA (Fig.  
226 3f), suggesting the degree of seed abortion is likely due to the levels of transgene expression. We  
227 next tested whether expression of *nDME<sup>CTD</sup>* or *DME<sup>FL</sup>* in WT Col-0 can also induce seed  
228 abortion phenotype. For each construct, more than 25 independent transgenic lines were  
229 examined and none resulted in any seed abortion phenotype (Supplementary Table 3). Thus the  
230 dominant negative effect appears to be specific to the DME NTD region.

231

### 232 **Evolutionary history and late acquisition of the N-terminal region of DME-like proteins.**

233 We show the C-terminal half of DME is sufficient to complement *dme* mutant developmental  
234 phenotypes, and can be recruited to most of the DME target loci. Thus the *DME<sup>CTD</sup>* most likely  
235 contains intrinsic targeting information. To gain insights from the evolution of the conserved  
236 domains in DME, we conducted sequence searches of the NR database with various homologs as  
237 query. The core of the DME-like proteins, as previously reported <sup>36</sup>, comprises the catalytic  
238 glycosylase domain of the HhH (helix-hairpin-helix) modules followed by the FCL ([Fe4S4]  
239 cluster loop) motif and a divergent version of an RRM (RNA Recognition Motif) fold domain  
240 (Fig. 4). The DNA glycosylase and FCL domains span the A and G regions, whereas the RRM  
241 fold domain corresponds to the B region of angiosperm DME homologs. A diversity of domains  
242 associate with the basic DME core can be found across various clades. Land plants and

243 charophytes (Streptophyta) possess a permuted divergent version of the unmethylated CpG  
244 recognizing CXXC domain (containing only one of two structural repeats of the classical CXXC  
245 domain) between the FCL and RRM domains. By contrast, one or more copies of the CXXC  
246 domain can be found in chlorophyte and stramenopile algae at distinct positions. Some algal  
247 DME homologs (from Chlorophyte and stramenopile) also possess other chromatin-modification  
248 reader (Tudor and PHD domains), DNA binding (AT-hook motif), and the DnaJ domain which  
249 interacts with the chaperone Hsp70<sup>36, 37</sup>. These accessory domains suggest a potential role for  
250 regulating the associated DNA glycosylase activity according to the DNA methylation (via  
251 CXXC) or chromatin status (via PHD, Tudor) of the cell in which they are expressed.

252 The N-terminal half of the DME consists of a large portion of unstructured, low complexity  
253 sequences (residues 346-947), a stretch of basic amino acid-rich direct repeats (residues 291-  
254 345), and a 120 amino-acid N-terminal domain (DemeN) of unknown function (residues 1-  
255 120)(see Supplementary Fig. 7 for sequence alignment). The DemeN domain and charged  
256 repeats are restricted to the angiosperm lineage and appears to be a late acquisition during land  
257 plant evolution.

258 In summary, the evolutionary history of the DME domains can be summarized as follows:  
259 bacterial versions of the HhH-FCL pair from a cyanobacterial source fused to an RRM-fold  
260 domain and further acquired an insert in the glycosylase domain to give the ancestral form in the  
261 plant lineage. This was likely then transferred to the stramenopiles from a secondary chlorophyte  
262 endosymbiont of this lineage. Finally, at the base of the streptophyte radiation, DME acquired a  
263 permuted CXXC, and later the DemeN domain and the associated charged repeats were acquired  
264 in the angiosperm lineage, possibly to facilitate and ensure a robust and thorough demethylation.

265

## 266 Discussion

267 We show for the first time that the core conserved region of the DME protein containing the  
268 DNA-glycosylase, FCL, divergent and permuted CXXC and divergent RRM domains is  
269 sufficient to rescue visible phenotypic defects caused by *dme* mutation. Although this truncated  
270 form of DME protein demethylates the majority of the canonical DME target sites, it does so in a  
271 less active and less efficient manner compared to the endogenous protein. We see two  
272 possibilities that might explain this lower activity and efficiency: 1) Critical cis-elements  
273 residing within introns or in 3'-end flanking sequences that are missing in the transgene might be  
274 required for robust transgene expression. 2) The N-terminal region might be required for full  
275 DME activity *in vivo*. Unfortunately, our attempt to assess the difference between DME<sup>FL</sup> and  
276 nDME<sup>CTD</sup> was confounded by the possible interference from truncated NTD proteins due to T-  
277 DNA insertion in *dme-2* background. We suspect this might contribute to the reduced DMRs  
278 observed in DME<sup>FL</sup>-complemented endosperm. Therefore, we believe it is premature to draw any  
279 conclusion based on direct comparisons between DME<sup>FL</sup>- and nDME<sup>CTD</sup>-complemented  
280 endosperm methylomes (Fig. 2c).

281 Since the C-terminal AGB region is sufficient for DME's seed viability function in *planta*,  
282 and can be recruited to most of the canonical DME target sites, the CTD polypeptide most likely  
283 contains sufficient targeting information. *in vitro* studies of ROS1 suggest that the B region  
284 containing the CXXC and RRM domains is essential for the glycosylase and lyase activities, and  
285 might recognize modified DNA<sup>38</sup>. It is possible that the permuted CXXC domain is required to  
286 direct the protein to the target sites, or is involved in discriminating methylated vs un-methylated  
287 cytosines<sup>39</sup>. This is supported by mutation studies that implicate a potential role for this domain  
288 in DME *in vivo* function, but not *in vitro* enzymatic activity (Huh and Hsieh, unpublished

289 results). Similarly, the role of the enigmatic divergent RNA-recognition motif (RRM) domain is  
290 also not fully understood. Mutagenesis screens for residues required for demethylation activity in  
291 bacteria identified multiple amino acid residues within the RRM domain<sup>40</sup>. Although the  
292 involvement of RNA species in the active DNA demethylation process has not been firmly  
293 established, an RRM protein ROS3 required for ROS1 demethylation suggests a potential role of  
294 non-coding RNAs in the active DNA demethylation pathway in Arabidopsis<sup>41</sup>. While it is  
295 tempting to speculate a role for RNA-binding, the DME RRM might also bind single-stranded  
296 DNA with methylated bases.

297 Based on the reduced demethylation activity of nDME<sup>CTD</sup> on the canonical DME target sites,  
298 we suspect the NTD region might be required for full and robust demethylation activity probably  
299 to ensure that the imprinting network is properly activated and maintained (e.g., by subsequent  
300 PRC2 activity). To achieve this, the DME NTD might function to assist the glycosylase enzyme  
301 by tightly binding to DNA template for more complete and thorough demethylation. Supporting  
302 such model, *in vitro* study of ROS1 activity on 5mC excision revealed that the basic repeats  
303 (3DR, AT-hooks) region binds strongly to DNA template non-specifically, and removal of NTD  
304 region impairs the sliding capacity of the protein on DNA template<sup>42</sup>, and significantly reduced  
305 ROS1 5mC excision activity<sup>43</sup>. We observed reduced degree of demethylation by nDME<sup>CTD</sup>  
306 regardless of target length (Supplemental Fig. 8), suggesting that NTD is needed for complete  
307 demethylation in all the target sites.

308 Although DME preferentially targets smaller euchromatic transposons that flank coding  
309 genes, it also targets gene-poor heterochromatin regions for demethylation<sup>13</sup>. The biological  
310 significance of heterochromatin demethylation by DME is not known, but was speculated to  
311 involve reinforcing DNA methylation in egg cell and subsequently in the embryo<sup>13</sup>. These

312 heterochromatin target sites are densely methylated, and demethylation by DME results in longer  
313 DMRs between *dme-2* and wt endosperm. Interestingly, the number of longer DMRs is  
314 significantly reduced between *dme-2* and *nDME<sup>CTD</sup>*-complemented endosperm, suggesting that  
315 removal of NTD region also reduces the processivity of demethylation in long target sites  
316 (Supplemental Fig. 9a). Since heterochromatin regions are compacted, demethylation in such  
317 loci will require substantial chromatin remodeling such as eviction of nucleosomes for DME to  
318 gain access to the templates. It is tempting to speculate that the conserved motif in the DemeN  
319 domain might recruit other factor(s) via protein interaction to remodel local chromatins to permit  
320 DME demethylation. However, based on current data we cannot unequivocally ascribe NTD's  
321 function due to lack of proper full length DME transgenic comparison. Nevertheless, our results  
322 caution that peculiarity in certain genetic backgrounds (e.g., *dme-2*) might confound data  
323 interpretation. Future work on DME functional study could benefit from the generation of a  
324 clean loss-of-function background such as deleting the entire DME locus using CRISPR-assisted  
325 genome editing techniques.

326 We envision a possible model where the AGB region is sufficient for directing DME to target  
327 loci while NTD region is required for interacting with local chromatin environment, stabilizing  
328 binding to chromosomal templates, and assisting demethylating flanking sequences. In the  
329 absence of NTD, *nDME<sup>CTD</sup>* can still demethylate majority of target sites, but in a less-efficient  
330 manner, likely due to the lack of non-specific DNA-binding by the basic AT-hook motifs. We  
331 surveyed wt DMRs that are longer than 1.5 kb, and found that these regions are also *nDME<sup>CTD</sup>*'s  
332 DMRs, but are shorter in length (Supplemental Fig. 9b), possibly due to missing the DemeN  
333 domain. If NTD is needed for longer and more robust demethylation, why ectopic expression of  
334 NTD causes dominant negative (DN) effects on endogenous protein? Classical examples of



335 dominant negative mutation often involve protein-protein interactions that are disrupted by  
336 mutated or truncated form of one particular partner or subunit. Although we do not have any  
337 evidence to suggest DME might homodimerize to become active, any weak physical interaction  
338 caused by ectopic NTD expression might induce conformational change that renders DME non-  
339 functional. Unfortunately our attempt to assess whether the NTD of DME can interact with each  
340 other was confounded by the self-activating activity of DME.2 NTD in yeast two-hybrid assay  
341 when fused to the GAL4 DNA binding domain (data not shown). Their possible interaction will  
342 need to be assessed by alternative strategies. Another possibility is that NTD binds and titrates  
343 out an important interacting partner required to activate DME through conformational change  
344 (allosteric interaction). By removing NTD, the AGB region is liberated from such  
345 conformational constrain and can demethylate its target sites. It is also possible that the non-  
346 specific DNA binding activity of NTD competes with DME for target sites, thereby reducing the  
347 overall efficiency of DME. The molecular underpinning of how NTD induces DN effect remains  
348 to be elucidated. From an evolutionary viewpoint, the use of an active DME-based  
349 demethylation appears to have been acquired early in the plant lineage. The presence of several  
350 accessory domains in addition to the conserved core suggests adjustments to the chromatin and  
351 methylation environment of the different species. The presence of additional domains such as the  
352 DemeN and basic repeats in angiosperms and the permuted CXXC domain in streptophyta  
353 lineage might reflect the adjustment to the unique methylation and chromatin environment of the  
354 larger Streptophyta and land plant genomes.

355

## 356 **Materials and Methods**

### 357 **Molecular Cloning of Constructs Used in this Study.**

358 All general molecular manipulations followed standard procedures (Sambrook et al. 1989). Q5  
359 High Fidelity DNA polymerase (NEB, Ipswich MA, USA) was used for PCR amplifications.  
360 PCR products were purified using AMPure XP beads (Beckman Coulter, Indianapolis IN, USA).  
361 The sequences of all plasmid constructs were confirmed by sequencing (Eton, Research Triangle  
362 Park NC, USA). All PCR primers and double-stranded DNA fragments were synthesized by  
363 Integrated DNA Technologies (Coralville IA, USA), and sequences are listed in Supplementary  
364 File 1.

365 A binary plasmid vector, pFGAMh, was modified to facilitate the generation of plasmid  
366 constructs using the Gibson assembly method. In brief, the replication origins and T-DNA  
367 borders originated from pFGC5941 (GenBank Accession: AY310901). A hygromycin resistance  
368 gene (HPTII) under the control of the mannopine synthase promoter was installed for selection  
369 of transgenic seedlings. A Gateway attR cassette (rfa, Invitrogen, Carlsbad CA, USA), flanked  
370 with unique restriction sites XhoI and XbaI-SpeI was placed upstream octopine synthase  
371 polyadenylation signal (OCS3'). Plasmid pFGAMh, digested with restriction enzymes XhoI and  
372 XbaI, was used to generate plasmids pDME:DME<sup>CTD</sup>, pDME:nDME<sup>CTD</sup> and  
373 pDME:GFP::DME<sup>CTD</sup> using the Gibson assembly method. The DME.2 upstream regulatory  
374 sequence (DMEpro; 2895 bp upstream of DME.2 translation start codon ATG) was PCR-  
375 amplified using primer pair VeDME/P3R and Col-0 gDNA as template. The coding sequence of  
376 linker-AGB (with a 6-Ala linker to its N-terminus; 3174 bp), was PCR-amplified using primer  
377 pair lnAGBF/CTDVeR and Col-0 cDNA as template. To bridge these two fragments (DMEpro  
378 and linker-AGB), one of the following three DNA fragments was used in the assembly reactions.  
379 For pDME:DME<sup>CTD</sup>, a 50-bp fragment was generated by annealing DNA oligos ATGF and  
380 ATGR. For pDME:SV40NLS::AGB, a 71-bp fragment was generated by annealing DNA oligos

381 S40F and S40R followed by two rounds of PCR reactions. For pDME:GFP::DME<sup>CTD</sup>, a 761-bp  
382 fragment was PCR-amplified using primer pair p3GFPF/dmGFPR and plasmid DNA pGFP-JS  
383 (Jen Sheen, Massachusetts General Hospital, Boston MA, USA) as template.

384 An intermediate plasmid vector, DME-P3-attR-AGB, was generated by digesting plasmid  
385 pDME:SV40NLS::AGB with restriction enzymes AflIII and NcoI, and re-assembled with a 2800-  
386 bp fragment, which was produced through overlap PCR with 3 primer pairs, upAflIII/P3attR,  
387 P3attF/attAGBR and attAGBF/dnNcoI, and Col-0 gDNA, attR cassette and Col-0 cDNA as  
388 templates. The resulting plasmid DME-P3-attR-AGB bears (1) the same 2895-bp regulatory  
389 sequence as the above constructs, (2) an attR cassette flanked by unique restrict sites XbaI and  
390 BglII, and (3) AGB coding sequence (3156 bp). To generate pDME:DME<sup>FL</sup>, plasmid DME-P3-  
391 attR-AGB was digested with XbaI and BglII, and assembled with a 2985-bp sequence, which  
392 was generated through overlap PCR using primer pairs S1-5e/IN3R and IN3F/S1-5R, and Col-0  
393 gDNA as template. The resulting plasmid pDME:DME<sup>FL</sup> carries the complete DME.2 coding  
394 sequence and intron 2 sequence (6075 bp) immediately downstream of the 2895-bp regulatory  
395 sequence with no additional sequences.

396 The intermediate plasmid vector DME-P3-attR-AGB was digested with restriction enzymes  
397 BglII and SpeI (to completely remove the AGB coding sequence), and re-assembled with a 786-  
398 bp sequence, which included the coding sequence of GFP (with its start codon ATG changed to  
399 TTG) and was PCR-amplified using primers ttGFPF and SpeGFPR and plasmid DNA pGFP-JS  
400 as template. The resulting plasmid DME-P3-attR-GFP was used as an intermediate plasmid  
401 vector to generate constructs pDME:DME<sup>NTD</sup>::GFP and pDME:mDME<sup>NTD</sup>::GFP. Plasmid DME-  
402 P3-attR-GFP was digested with XbaI and BglII, and assembled with two DNA fragments: a  
403 3289-bp sequence was PCR-amplified using primers S1-5F and dme2tR2 and Col-0 gDNA as

404 template and a 158-bp synthetic DNA fragment (FragQ20) (Integrated DNA Technologies,  
405 Coralville IA, USA). The resulting construct pDME:DME<sup>NTD</sup>::GFP included the 2895-bp  
406 upstream regulatory sequence, the 3332-bp sequence downstream of translation start codon ATG,  
407 the coding sequence of 6-Ala linker, and the coding sequence of GFP. Note the NTD coding  
408 sequence included the first 86 bp of intron 4 of gene DME.2, and it was designed to mimic dme-  
409 2 T-DNA insertion. To generate pDME:mDME<sup>NTD</sup>::GFP, the sequence of the first 1012 amino  
410 acid residues of DME.2 protein was converted to DNA sequence using program EMBOSS  
411 Backtranseq ([http://www.ebi.ac.uk/Tools/st/emboss\\_backtranseq/](http://www.ebi.ac.uk/Tools/st/emboss_backtranseq/)) and the Homo sapiens codon  
412 usage table. The sequence was then analyzed using online programs SoftBerry FSPLICE  
413 (<http://linux1.softberry.com/berry.phtml?topic=fsplice&group=programs&subgroup=gfind>) and  
414 NetPlantGene2 (<http://www.cbs.dtu.dk/services/NetPGene/>), and manually edited to disrupt  
415 potential splicing donor sites or acceptor sites. The mDME<sup>NTD</sup> sequence (3036 bp) and upstream-  
416 and downstream-overlapping sequence are broken into 4 fragments, and synthesized by  
417 Integrated DNA Technologies (Coralville IA, USA). The 4 DNA fragments were assembled with  
418 plasmid DME-P3-attR-GFP digested with XbaI and BglII, resulting construct  
419 pDME:mNTDh::GFP.

420

#### 421 **Whole-Genome Bisulfite Sequencing and DNA Methylation Analysis**

422 Genomic DNA were isolated from hand dissected, 7-9 DAP *dme-2* endosperm that has been  
423 complemented by *DME<sup>FL</sup>* or *nDME<sup>CTD</sup>* (*dme-2/dme-2;DME<sup>FL</sup>/DME<sup>FL</sup>* or *dme-2/dme-2;*  
424 *nDME<sup>CTD</sup> nDME<sup>CTD</sup>*). Whole genome bisulfite sequencing library was constructed as described  
425 before<sup>13, 44</sup>. Approximately 20-50 ng of purified genomic DNA was spiked with 0.5ng of  
426 unmethylated cl857 *Sam7* Lambda DNA (Promega, Madison, WI) and sheared to about 300bp

427 using Covaris M220 (Covaris Inc., Woburn, Massachusetts) under the following settings: target  
428 BP, 300; peak incident power, 75 W; duty factor, 10%; cycles per burst, 200; treatment time, 90  
429 second; sample volume 50 $\mu$ l. The sheared DNA was cleaned up and recovered by 1.2x AMPure  
430 XP beads then followed by end repaired and A-tailing (NEBNext Ultra II DNA Library Prep Kit  
431 for Illumina, NEB) before ligation to NEBNext methylated multiplex adapters (NEBNext  
432 Multiplex Oligos for Illumina, NEB) according to the manufacturer's instructions. Adaptor-  
433 ligated DNA was cleaned up with 1x AMPure XP beads. The purified adaptor-ligated DNA was  
434 spiked with 50ng of unmethylated cl857 *Sam7* Lambda DNA and subjected to one round of  
435 sodium bisulfite conversion using the EZ DNA Methylation-Lightning Kit (Zymo Research  
436 Corporation, Irvine, CA) as outlined in the manufacturer's instructions with 80 min of incubation  
437 time. Half of the bisulfite-converted DNA molecules was PCR amplified with the following  
438 condition: 2.5 U of ExTaq DNA polymerase (Takara), 5 ul of 10 x Extaq reaction buffer, 25  $\mu$ M  
439 dNTPs, 1 ul of index Primers (10  $\mu$ M) in 50 uL reaction. The thermocycling condition was as  
440 follows: 95 °C for 2 min and then 10 cycles each of 95 °C for 30 s, 65 °C for 30 s, and 72 °C for  
441 60 s. The enriched libraries were purified twice with 0.8x (v/v) AMPure XP beads to remove any  
442 adapter dimers. High throughput sequencing was performed by Novogene Corporation (USA).  
443 For each genotype, sequencing reads from three individual transgenic lines were combined.  
444 Sequenced reads were mapped to the TAIR10 reference genomes and DNA methylation analyses  
445 were performed as previously described (Supplementary Table 7)<sup>13</sup>. Fractional CG methylation  
446 in 50-bp windows across the genome was compared between *dme*, wild-type (GSE38935<sup>13</sup>),  
447 *DME<sup>FL</sup>*- *nDME<sup>CTD</sup>*- complemented *dme-2* endosperm. Windows with a fractional CG  
448 methylation difference of at least 0.3 in the endosperm comparison (Fisher's exact test p-value <  
449 0.001) were merged to generate larger differentially methylated regions (DMRs) if they occurred

450 within 300 bp. DMRs were retained for further analysis if the fractional CG methylation across  
451 the whole DMR was 0.3 greater in *dme* endosperm than in wild-type endosperm (Fisher's exact  
452 test p-value  $< 10^{-10}$ ), and if the DMR is at least 100-bp long. The merged DMR lists are in the  
453 Supplemental File 2. The *dme* and wild-type endosperm data used in this study were derived  
454 from crossed between *Col* (female parent) and *Ler* (male parent) (GSE38935, <sup>13</sup>). To avoid  
455 potential ecotype-specific methylation difference, *Ler* hyper-DMRs relative to Col-0 endosperms  
456 (GSE52814, <sup>45</sup>) were identified using the same criteria as described above and excluded from  
457 further analyses. For making the Venn diagram, merged DMR regions were converted into 50-bp  
458 windows. Only windows with methylation scores in all samples were retained for comparison in  
459 Venn diagram and boxplot analysis.

460

#### 461 **Plant Materials and Complementation Assays**

462 We found we can easily obtained *dme-2/dme-2 Col-gl* plants from *DME/dme-2* heterozygotes if  
463 we rescued seeds prior to desiccation on MS sucrose plates. This is consistent with the report that  
464 *fis* endosperm cellularization defect and embryo arrest can be rescued by culturing the  
465 developing seeds in sucrose media because *fis* seeds have reduced hexose level <sup>46</sup>. Using this  
466 method we generated multiple homozygous lines, and we did not detect any difference between  
467 individuals in terms of normal seed rate or visible phenotype. The adult *dme-2/dme-2* plants are  
468 morphologically indistinguishable from wild-type *Col-gl* plants but produce ~0.1% viable  
469 mature seeds. These *dme-2/dme-2* plants are not due to genetic mutation or heritable aberrant  
470 epigenetic effects that escape requirement of DME activity during gametogenesis because their  
471 subsequent progeny are phenotypically normal and produces same level (~0.1%) of normal seeds.

472 The *DME/dme-2* heterozygous or *dme-2/dme-2* homozygous lines in *Col-gl* background were  
473 subjected to Agrobacterium-mediated floral dipping transformation procedures<sup>28</sup>. Seeds were  
474 sterilized by 30% bleach solution and screened for T1 transgenic plants on a 0.5x MS nutrient  
475 medium with 1% sucrose, 0.8% agar and 40 µg/ml hygromycin. Germinated seedlings were  
476 transferred to soil and grown in the growth room under 16 hours of light and 8 hours of dark  
477 cycles at 23°C. Siliques from T1 transgenic plants were dissected 14-16 days after self-  
478 pollination using a stereoscopic microscope (SteREO Discovery.V12, Carl Zeiss, Wetzlar,  
479 Germany). The numbers of viable and aborted seeds in transgenic lines were statistically  
480 analyzed with the  $\chi^2$  test. The probability that deviates from a 1:1 or 3:1 segregation ratio for  
481 viable and aborted seeds was also calculated.

482

### 483 **RNA extraction, cDNA synthesis and quantitative PCR analysis**

484 Total RNA was extracted using TRIzol® Reagent (Invitrogen, Carlsbad, USA) and treated with  
485 TURBO DNase (Ambion, Austin TX, USA) according to the manufacturers' instructions. For  
486 cDNA synthesis, 5mg of total RNA was reverse-transcribed using Superscript III Reverse  
487 Transcriptase and oligo(dT) primer (Invitrogen). The cDNA was treated with RNase H  
488 (Invitrogen) at 37°C for 20min and diluted tenfold with H<sub>2</sub>O. For each 15-µl qPCR reaction, 1µl  
489 of diluted cDNA was used. The quantitative PCR was run on ABI 7500 Fast Real-Time PCR  
490 System (<http://www.appliedbiosystems.com>) using FastStart Universal SYBR Green Master Mix  
491 (Roche, <http://www.roche.com>). The quantitative PCR primers are listed in Supplementary File 1.  
492 The Ct values were normalized against *ACT2* (*At3g18780*) mRNA or *UBC* (*At5g25760*) mRNA.  
493 The abundance of mRNAs was expressed as relative to controls, with control values set to 1. The  
494 error bars represent the standard deviation of 4 biological replicates.

495

496 **Protein domain analysis and phylogenetic inference**

497 We utilized a domain-centric computational strategy to study DME and its related proteins.  
498 Specifically, we identify DME homologs by using the iterative profile searches with PSI-BLAST  
499 <sup>47</sup> from the protein non-redundant (NR) database at National Center for Biotechnology  
500 Information (NCBI). Multiple sequence alignments were built by the Promals <sup>48</sup> program,  
501 followed by careful manual adjustments. Consensus secondary structures were predicted using  
502 the PSIPRED <sup>49</sup> JPred program <sup>50</sup>. Conserved domains were further characterized based on the  
503 comparison to available domain models from pfam <sup>51</sup> and sequence/structural features. The  
504 PhyML program <sup>52</sup> was used to determine the maximum-likelihood tree using the Jones–Taylor–  
505 Thornton (JTT) model for amino acids substitution with a discrete gamma model (four categories  
506 with gamma shape parameter: 1.096). The tree was rendered using MEGA Tree Explorer <sup>53</sup>.

507

508 **Acknowledgments**

509 We thank Drs. Ping-Hung Hsieh and Jer-Young Lin for assistance in methylome analysis, Robert  
510 Goldberg, Robert Fischer and Matthew Bauer for discussions during the course of this study.  
511 This work is partially supported by the Hatch Project 02413 (to T.-F.H.), National Institute of  
512 Food and Agriculture, U.S. Department of Agriculture, U.S.A., by the National Science  
513 Foundation Grant MCB-1715115 to T.-F.H. and W.Y.X., and by the State of NC appropriations  
514 as distributed by the University of North Carolina General Administration and the NC  
515 Agricultural Research Service Office at NC State University. LMI and LA are supported by the  
516 Intramural Research Program of the National Library of Medicine, NIH, USA.

517 **Author contribution.**



518 C.Z., Y.-H.H., X.-Q.Z., J.H.H. and T.-F.H. designed the research. C.Z., Y.-H.H., X.-Q.Z.  
519 performed the experiments. D.Z., L.M.I, and L.A. performed the evolutionary analysis. C.Z., Y.-  
520 H.H., and T.-F.H. wrote the article. T.-F.H., C.Z., Y.-H.H., W.X., J.H.H. interpreted and  
521 commented the article.

## 522 **References**

- 523 1. Yang WC, Shi DQ, Chen YH. Female gametophyte development in flowering  
524 plants. *Annu Rev Plant Biol* **61**, 89-108 (2010).  
525
- 526 2. Gehring M. Genomic imprinting: insights from plants. *Annu Rev Genet* **47**, 187-  
527 208 (2013).  
528
- 529 3. Kohler C, Wolff P, Spillane C. Epigenetic mechanisms underlying genomic  
530 imprinting in plants. *Annu Rev Plant Biol* **63**, 331-352 (2012).  
531
- 532 4. Jullien PE, Kinoshita T, Ohad N, Berger F. Maintenance of DNA Methylation  
533 during the Arabidopsis Life Cycle Is Essential for Parental Imprinting. *Plant Cell*  
534 **18**, 1360-1372 (2006).  
535
- 536 5. Gehring M, *et al.* DEMETER DNA glycosylase establishes MEDEA polycomb  
537 gene self-imprinting by allele-specific demethylation. *Cell* **124**, 495-506 (2006).  
538
- 539 6. Xiao W, *et al.* Imprinting of the MEA Polycomb gene is controlled by antagonism  
540 between MET1 methyltransferase and DME glycosylase. *Dev Cell* **5**, 891-901  
541 (2003).  
542
- 543 7. Kinoshita T, *et al.* One-way control of FWA imprinting in Arabidopsis endosperm  
544 by DNA methylation. *Science* **303**, 521-523 (2004).  
545

- 546 8. Tiwari S, *et al.* MATERNALLY EXPRESSED PAB C-TERMINAL, a novel  
547 imprinted gene in Arabidopsis, encodes the conserved C-terminal domain of  
548 polyadenylate binding proteins. *Plant Cell* **20**, 2387-2398 (2008).  
549
- 550 9. Choi Y, *et al.* DEMETER, a DNA Glycosylase Domain Protein, Is Required for  
551 Endosperm Gene Imprinting and Seed Viability in *Arabidopsis*. *Cell* **110**, 33-42  
552 (2002).  
553
- 554 10. Penterman J, Zilberman D, Huh JH, Ballinger T, Henikoff S, Fischer RL. DNA  
555 demethylation in the Arabidopsis genome. *Proceedings of the National Academy  
556 of Sciences of the United States of America* **104**, 6752-6757 (2007).  
557
- 558 11. Lister R, *et al.* Highly integrated single-base resolution maps of the Arabidopsis  
559 genome. *Cell* **133**, 395-397 (2008).  
560
- 561 12. Gong Z, Morales-Ruiz T, Ariza RR, Roldan-Arjona T, David L, Zhu J-K. ROS1, a  
562 Repressor of Transcriptional Gene Silencing in Arabidopsis, Encodes a DNA  
563 Glycosylase/Lyase. *Cell* **111**, 803-814 (2002).  
564
- 565 13. Ibarra CA, *et al.* Active DNA demethylation in plant companion cells reinforces  
566 transposon methylation in gametes. *Science* **337**, 1360-1364 (2012).  
567
- 568 14. Hsieh TF, *et al.* Regulation of imprinted gene expression in Arabidopsis  
569 endosperm. *Proceedings of the National Academy of Sciences of the United  
570 States of America* **108**, 1755-1762 (2011).  
571
- 572 15. Hsieh TF, *et al.* Genome-wide demethylation of Arabidopsis endosperm. *Science*  
573 **324**, 1451-1454 (2009).  
574
- 575 16. Wang X, *et al.* RNA-binding protein regulates plant DNA methylation by

- 576 controlling mRNA processing at the intronic heterochromatin-containing gene  
577 IBM1. *Proceedings of the National Academy of Sciences of the United States of*  
578 *America* **110**, 15467-15472 (2013).
- 579
- 580 17. Lei M, Zhang H, Julian R, Tang K, Xie S, Zhu JK. Regulatory link between DNA  
581 methylation and active demethylation in Arabidopsis. *Proceedings of the National*  
582 *Academy of Sciences of the United States of America* **112**, 3553-3557 (2015).
- 583
- 584 18. Lang Z, *et al.* The methyl-CpG-binding protein MBD7 facilitates active DNA  
585 demethylation to limit DNA hyper-methylation and transcriptional gene silencing.  
586 *Mol Cell* **57**, 971-983 (2015).
- 587
- 588 19. Qian W, *et al.* A histone acetyltransferase regulates active DNA demethylation in  
589 Arabidopsis. *Science* **336**, 1445-1448 (2012).
- 590
- 591 20. Ikeda Y, *et al.* HMG domain containing SSRP1 is required for DNA demethylation  
592 and genomic imprinting in Arabidopsis. *Dev Cell* **21**, 589-596 (2011).
- 593
- 594 21. Bustin M, Catez F, Lim JH. The dynamics of histone H1 function in chromatin.  
595 *Mol Cell* **17**, 617-620 (2005).
- 596
- 597 22. Fan Y, *et al.* Histone H1 depletion in mammals alters global chromatin structure  
598 but causes specific changes in gene regulation. *Cell* **123**, 1199-1212 (2005).
- 599
- 600 23. Graziano V, Gerchman SE, Schneider DK, Ramakrishnan V. Histone H1 is  
601 located in the interior of the chromatin 30-nm filament. *Nature* **368**, 351-354  
602 (1994).
- 603
- 604 24. Hashimoto H, *et al.* Histone H1 null vertebrate cells exhibit altered nucleosome  
605 architecture. *Nucleic Acids Res* **38**, 3533-3545 (2010).

- 606
- 607 25. Rea M, *et al.* Histone H1 affects gene imprinting and DNA methylation in  
608 *Arabidopsis*. *Plant J* **71**, 776-786 (2012).
- 609
- 610 26. Brooks SC, Fischer RL, Huh JH, Eichman BF. 5-methylcytosine recognition by  
611 *Arabidopsis thaliana* DNA glycosylases DEMETER and DML3. *Biochemistry* **53**,  
612 2525-2532 (2014).
- 613
- 614 27. Jang H, Shin H, Eichman BF, Huh JH. Excision of 5-hydroxymethylcytosine by  
615 DEMETER family DNA glycosylases. *Biochem Biophys Res Commun* **446**, 1067-  
616 1072 (2014).
- 617
- 618 28. Clough SJ, Bent AF. Floral dip: a simplified method for *Agrobacterium*-mediated  
619 transformation of *Arabidopsis thaliana*. *Plant J* **16**, 735-743 (1998).
- 620
- 621 29. Park JS, *et al.* Control of DEMETER DNA demethylase gene transcription in  
622 male and female gamete companion cells in *Arabidopsis thaliana*. *Proceedings*  
623 *of the National Academy of Sciences of the United States of America* **114**, 2078-  
624 2083 (2017).
- 625
- 626 30. Kohler C, Hennig L, Bouveret R, Gheyselinck J, Grossniklaus U, Grissem W.  
627 *Arabidopsis* MSI1 is a component of the MEA/FIE Polycomb group complex and  
628 required for seed development. *The EMBO journal* **22**, 4804-4814 (2003).
- 629
- 630 31. Grossniklaus U, Vielle-Calzada J-P, Hoepfner MA, Gagliano WB. Maternal  
631 control of embryogenesis by *MEDEA*, a polycomb-group gene in *Arabidopsis*.  
632 *Science* **280**, 446-450 (1998).
- 633
- 634 32. Luo M, Bilodeau P, Dennis ES, Peacock WJ, Chaudhury A. Expression and  
635 parent-of-origin effects for FIS2, MEA, and FIE in the endosperm and embryo of

- 636 developing *Arabidopsis* seeds. *Proceedings of the National Academy of*  
637 *Sciences of the United States of America* **97**, 10637-10642 (2000).
- 638
- 639 33. Schoft VK, *et al.* Function of the DEMETER DNA glycosylase in the *Arabidopsis*  
640 *thaliana* male gametophyte. *Proceedings of the National Academy of Sciences of*  
641 *the United States of America* **108**, 8042-8047 (2011).
- 642
- 643 34. Lang Z, *et al.* Critical roles of DNA demethylation in the activation of ripening-  
644 induced genes and inhibition of ripening-repressed genes in tomato fruit.  
645 *Proceedings of the National Academy of Sciences of the United States of*  
646 *America* **114**, E4511-E4519 (2017).
- 647
- 648 35. Choi Y, Harada JJ, Goldberg RB, Fischer RL. An invariant aspartic acid in the  
649 DNA glycosylase domain of DEMETER is necessary for transcriptional activation  
650 of the imprinted MEDEA gene. *Proceedings of the National Academy of Sciences*  
651 *of the United States of America* **101**, 7481-7486 (2004).
- 652
- 653 36. Iyer LM, Abhiman S, Aravind L. Natural history of eukaryotic DNA methylation  
654 systems. *Progress in molecular biology and translational science* **101**, 25-104  
655 (2011).
- 656
- 657 37. Walsh P, Bursac D, Law YC, Cyr D, Lithgow T. The J-protein family: modulating  
658 protein assembly, disassembly and translocation. *EMBO reports* **5**, 567-571  
659 (2004).
- 660
- 661 38. Hong S, Hashimoto H, Kow YW, Zhang X, Cheng X. The Carboxy-Terminal  
662 Domain of ROS1 Is Essential for 5-Methylcytosine DNA Glycosylase Activity. *J*  
663 *Mol Biol*, (2014).
- 664
- 665 39. Long HK, Blackledge NP, Klose RJ. ZF-CxxC domain-containing proteins, CpG

- 666 islands and the chromatin connection. *Biochem Soc Trans* **41**, 727-740 (2013).  
667
- 668 40. Mok YG, *et al.* Domain structure of the DEMETER 5-methylcytosine DNA  
669 glycosylase. *Proceedings of the National Academy of Sciences of the United*  
670 *States of America* **107**, 19225-19230 (2010).  
671
- 672 41. Zheng X, *et al.* ROS3 is an RNA-binding protein required for DNA demethylation  
673 in Arabidopsis. *Nature* **455**, 1259-1262 (2008).  
674
- 675 42. Ponferrada-Marin MI, Roldan-Arjona T, Ariza RR. Demethylation initiated by  
676 ROS1 glycosylase involves random sliding along DNA. *Nucleic Acids Res* **40**,  
677 11554-11562 (2012).  
678
- 679 43. Ponferrada-Marin MI, Martinez-Macias MI, Morales-Ruiz T, Roldan-Arjona T,  
680 Ariza RR. Methylation-independent DNA binding modulates specificity of  
681 Repressor of Silencing 1 (ROS1) and facilitates demethylation in long substrates.  
682 *The Journal of biological chemistry* **285**, 23032-23039 (2010).  
683
- 684 44. Hsieh TF. Whole-genome DNA methylation profiling with nucleotide resolution.  
685 *Methods in molecular biology* **1284**, 27-40 (2015).  
686
- 687 45. Pignatta D, Erdmann RM, Scheer E, Picard CL, Bell GW, Gehring M. Natural  
688 epigenetic polymorphisms lead to intraspecific variation in Arabidopsis gene  
689 imprinting. *Elife* **3**, e03198 (2014).  
690
- 691 46. Hehenberger E, Kradolfer D, Kohler C. Endosperm cellularization defines an  
692 important developmental transition for embryo development. *Development* **139**,  
693 2031-2039 (2012).  
694
- 695 47. Altschul SF, *et al.* Gapped BLAST and PSI-BLAST: a new generation of protein

- 696 database search programs. *Nucleic Acids Res* **25**, 3389-3402 (1997).
- 697
- 698 48. Pei J, Grishin NV. PROMALS: towards accurate multiple sequence alignments of  
699 distantly related proteins. *Bioinformatics* **23**, 802-808 (2007).
- 700
- 701 49. Buchan DW, Minneci F, Nugent TC, Bryson K, Jones DT. Scalable web services  
702 for the PSIPRED Protein Analysis Workbench. *Nucleic Acids Res* **41**, W349-357  
703 (2013).
- 704
- 705 50. Cuff JA, Clamp ME, Siddiqui AS, Finlay M, Barton GJ. JPred: a consensus  
706 secondary structure prediction server. *Bioinformatics* **14**, 892-893 (1998).
- 707
- 708 51. Finn RD, *et al.* The Pfam protein families database: towards a more sustainable  
709 future. *Nucleic Acids Res* **44**, D279-285 (2016).
- 710
- 711 52. Guindon S, Dufayard JF, Lefort V, Anisimova M, Hordijk W, Gascuel O. New  
712 algorithms and methods to estimate maximum-likelihood phylogenies: assessing  
713 the performance of PhyML 3.0. *Syst Biol* **59**, 307-321 (2010).
- 714
- 715 53. Tamura K, Dudley J, Nei M, Kumar S. MEGA4: Molecular Evolutionary Genetics  
716 Analysis (MEGA) software version 4.0. *Mol Biol Evol* **24**, 1596-1599 (2007).

717  
718  
719  
720  
721

## Figure Legends

### 722 **Figure 1 Complementation of *dme* seed abortion phenotype by the truncated DME nAGB.**

723 (a) Siliques were dissected and photographed 14 days after self-pollination. In *dme-2/dme-2*  
724 silique greater than 99% of seeds are aborted. A single copy of *nDME<sup>CTD</sup>* transgene reduces seed  
725 abortion rate to 50%; and in the *dme-2/dme-2; nDME<sup>CTD</sup>/nDME<sup>CTD</sup>* silique, all the *dme-2* seeds

726 are rescued and developed normally. Scale bar = 0.5 mm. (b) Complementation of *dme-2* seed  
727 abortion phenotype by *nDME<sup>CTD</sup>* and *DME<sup>FL</sup>*. (c) The *nDME<sup>CTD</sup>* transgene restores DME target  
728 genes *FWA* and *FIS2* expression. WT: Col-0; *nDME<sup>CTD</sup>*: *dme-2/dme-2*; *nDME<sup>CTD</sup>/nDME<sup>CTD</sup>*;  
729 *dme-2: dme-2/dme-2*. Total RNA was isolated from stage F1 to F12 floral buds.

730

731 **Figure 2 Endosperm methylome analysis.** (a) Genome browser snapshots of CG DNA  
732 methylation at selected imprinted gene loci. Top two tracks are coding genes (magenta) and TEs  
733 (orange) with Tair10 chromosome coordinates. For the bottom seven tracks, each track  
734 represents fractional CG methylation levels for different genotype: black trace, *dme-2* endosperm;  
735 dark green trace, WT endosperm; dark blue trace, *DME<sup>FL</sup>*-complemented endosperm; dark purple  
736 trace, *nDME<sup>CTD</sup>*-complemented endosperm; light green trace, WT endosperm subtracted from  
737 *dme-2* mutant endosperm; light blue trace, *DME<sup>FL</sup>*-complemented endosperm subtracted from  
738 *dme-2* endosperm; light purple trace, *nDME<sup>CTD</sup>*-complemented endosperm subtracted from  
739 *dme-2* endosperm. DNA CG hypomethylation at selected maternally expressed (*FIS2* and *SDC*) and  
740 paternally expressed (*SUV7*, *YUC10*, and *PHE1*) imprinted genes is restored in *DME<sup>FL</sup>*- and  
741 *nDME<sup>CTD</sup>*-complemented endosperm. (b) Boxplot of CG methylation levels among canonical  
742 DME target sites in *dme-2* mutant (grey), WT (white), *DME<sup>FL</sup>*- (blue), or *nDME<sup>CTD</sup>*- (red)  
743 complemented endosperm. (c) Venn Diagram (top panel) of CG hyper-DMRs in 50-bp windows  
744 between *dme-2* endosperm relative to WT, *DME<sup>FL</sup>*-complemented or *nDME<sup>CTD</sup>*-complemented  
745 endosperm. Boxplot (bottom panel) of CG methylation levels in *dme-2* mutant (grey), WT  
746 (white), *DME<sup>FL</sup>*- (blue) or *nDME<sup>CTD</sup>*- (red) complemented endosperm in WT only (left panel),  
747 *DME<sup>FL</sup>* only, or *nDME<sup>CTD</sup>* only (right panel) DMRs.

748



749 **Figure 3 Expression of DME NTD region in wild-type central cell induces *dme*-like seed**  
750 **abortion phenotype. (a)** Confocal microscopy image of ovule in F12 floral bud shows the  
751 expression of mDME<sup>NTD</sup>-GFP in the central cell. Scale bar, 20  $\mu$ m. **(b-c)** Ectopic expression of  
752 *DME*<sup>NTD</sup> in WT central cell induces *dme-2* like seed abortion phenotype in silique **(b)** and in  
753 developing seeds **(c)**. Total RNA was isolated from stage F1 to F12 floral buds from independent  
754 lines with different seed abortion ratios **(d)** to assess transgene and endogenous DME expression.  
755 **(e)** Endogenous DME transcript levels in independent transgenic lines are comparable to the  
756 control line, but the transgene expression level varies among these independent lines with  
757 different seed abortion rates. Error bars indicate SD. NS,  $p > 0.2$  (Ctrl vs 23),  $p > 0.5$  (Ctrl vs 15),  
758  $p > 0.3$  (Ctrl vs 25),  $p > 0.4$  (Ctrl vs 8), not significant (two-tailed t test). **(f)** Correlation analysis  
759 shows that the transcript abundance of the transgene, but not that of the endogenous DME  
760 transcripts, correlates with seed abortion rates (by linear regression).

761  
762 **Figure 4. Evolution of plant DME-like proteins.** A phylogenetic tree was reconstructed using  
763 the PhyML program. Only node supporting values  $> 0.80$  from ML bootstrap analyses are shown.  
764 The representative domain architectures of DME homologs in major plant clades are shown  
765 along the tree, demonstrating domain fusions during evolution. Domain abbreviations: DemeN,  
766 N-terminal domain of DEME-like proteins in angiosperms; DnaJ, DnaJ molecular chaperone  
767 homology domain (Pfam: PF00226); FCL, [Fe4S4] cluster loop motif (also called Iron-sulfur  
768 binding domain of endonuclease III; Pfam: PF10576); HhH-GL, HhH-GPD superfamily base  
769 excision DNA repair protein (Pfam: PF00730); PHD, PHD finger (Pfam: PF00628); RRM, RNA  
770 recognition motif (Pfam: PF00076); Tudor, Tudor domain (Pfam: PF00567).

771

772 **Supplemental Information**

773 **Figure Legends**

774 **Fig. S1. Diagrams of DME protein structure and transgene constructs.**

775 (a) DME protein domain architecture. The positions of conserved domains along DME protein.  
776 Numbers represent amino acid position relative to the translation start sites. DME.1 is shorter  
777 than DME.2 by 258 amino acids due to alternative splicing, missing the very N-terminal DemeN  
778 domain. DemeN is a domain of unknown function conserved among angiosperm DME-like  
779 protein. 3DR is the stretch of basic rich amino acid direct repeats, resembling AT-hook motifs,  
780 and serves as a nuclear localization signal; per-CXXC is the permuted CXXC zinc finger motif;  
781 RRM is the RNA recognition motif; FCL is a [Fe4S4] cluster loop following the HhH module.  
782 The *dme-2* allele harbors a T-DNA insertion in region A at amino acid position 1012. ID1 and  
783 ID2 are variable, low complexity sequences between the glycosylase domain and the conserved  
784 B region. (b) Transgene constructs used in this study. DMEpro refers to the upstream regulatory  
785 sequence (2895 bp upstream of the translation start codon ATG) of DME.2. SV40NLS:  
786 PKKKRKV. A polypeptide linker comprising 6 alanine residues is placed between any protein  
787 fragment fusions.

788

789 **Fig. S2. DNA methylomes of three independent *nDME<sup>CTD</sup>*-complemented *dme-2* endosperm.**

790 (a) Venn diagram showing partial overlap of *dme* CG hyper-DMRs relative to each nAGB-  
791 complemented endosperm (*nDME<sup>CTD</sup>-1* to *nDME<sup>CTD</sup>-3*). (b) Boxplot of CG methylation levels  
792 among canonical DME target sites in *dme-2* mutant (black), *nDME<sup>CTD</sup>-1* (pink), *nDME<sup>CTD</sup>-2*  
793 (magenta), or *nDME<sup>CTD</sup>-3* (red) complemented endosperm, in *nDME<sup>CTD</sup>-1* specific (left panel),  
794 *nDME<sup>CTD</sup>-2* specific (middle panel), and *nDME<sup>CTD</sup>-3* specific DMRs. These results show that the

795 combined DMRs are more or less hypomethylated in each independent line compared to *dme-2*  
796 endosperm.

797

798 **Fig. S3. DNA methylomes of three independent  $DME^{FL}$ -complemented *dme-2* endosperm.** (a)

799 Venn diagram showing partial-overlap of *dme* CG hyper-DMRs relatives to each  $DME^{FL}$ -

800 complemented endosperm ( $DME^{FL-1}$  to  $DME^{FL-3}$ ). (b) Boxplot of CG methylation levels among

801 canonical DME target sites in *dme-2* mutant (black),  $DME^{FL-1}$  (light blue),  $DME^{FL-2}$  (medium

802 blue), or  $DME^{FL-3}$  (dark blue) complemented endosperm, in  $DME^{FL-1}$  specific (left panel),

803  $DME^{FL-2}$  specific (middle panel), and  $DME^{FL-3}$  specific DMRs. These results show that the

804 combined DMRs are more or less hypomethylated in each independent line compared to *dme-2*

805 endosperm.

806

807 **Fig. S4. The DMRs of *dme* relative to WT endosperm or  $nDME^{CTD}$ - complemented**

808 **endosperm.** Venn Diagram (top) and Boxplot analysis (bottom) of CG hyper-DMRs in 50-bp

809 windows between *dme-2* endosperm relative to  $nDME^{CTD}$ -complemented or WT endosperm. CG

810 methylation levels of DMRs unique to  $nDME^{CTD}$ -complemented endosperm are also

811 demethylated in the WT endosperm (left panel). Similarly, DMRs unique to WT endosperm are

812 demethylated in  $nDME^{CTD}$ -complemented endosperm (right).

813

814 **Fig. S5.  $DME^{FL}$  and  $nDME^{CTD}$  transgenes are expressed at comparable levels among**

815 **independent complementation lines.**  $DME^{FL}$  and  $nDME^{CTD}$  expression levels are comparable

816 between the four of the six complementation lines used in the methylome study. Total RNA was

817 isolated from stage F1 to F12 floral buds. The results show that there is no significant difference

818 in expression level between these two transgenes(t-test,  $p>0.4$ ).

819

820 **Fig. S6. The effects of T-DNA insertion on endogenous DME transcript abundance in *dme-***  
821 ***2/dme-2* plants.** Total RNA was isolated from stage F1 to F12 floral buds. Equal amount of total  
822 RNA from WT and *dme-2/dme-2* were used for reverse transcription and quantitative PCR. Six  
823 paired of primers (PN1-PN6) correspond to the N-terminal region before the T-DNA insertion  
824 site, and three pairs of C-terminal region primers (PC1-PC3) were used to assess endogenous  
825 DME transcript level in *dme-2/dme-2* mutant plants. The position of each primer pair is indicated  
826 in the DME diagram where T-DNA insertion site is shown.

827

828 **Fig. S7. Alignment of angiosperm DME-like proteins showing the conserved DemeN**  
829 **domain and the basic rich 3DR repeats.** Bioinformatics analysis using available DME-like  
830 sequences identified a ~ 120-amino-acid-long conserved region at the very N-termini among  
831 DME-like proteins in angiosperms. This sequence is characterized by a highly conserved  
832 WxPxTPxK motif that might function in protein-protein interactions. Further toward the C-  
833 terminus is a stretch of basic amino acids rich region that serves as a nuclear localization signal.  
834 This sequence consists of three direct repeats (3DR) reminiscent of the AT-hook motifs that may  
835 bind DNA.

836

837 **Fig. S8. Boxplot of CG methylation levels among canonical DME target sites in different DMR**  
838 **length category, in *dme-2* mutant (black), wild-type (white), or *nDME<sup>CTD</sup>*-complemented**  
839 **endosperm**

840

841 **Fig. S9.** (a) Merged DMR length distribution in WT and *nDME<sup>CTD</sup>*-complemented endosperm. (b)  
842 Genome Browser examples of long WT DMRs. Tracks are as labeled. The DMR regions are  
843 indicated as horizontal bars according to their length in each sample (bottom two tracks). Even  
844 though *nDME<sup>CTD</sup>* complemented endosperm lack longer DMRs, these regions are also shorter  
845 DMRs in *nDME<sup>CTD</sup>*-complemented endosperm.  
846  
847  
848  
849

850 **Table 1. Rescue of the reduced paternal *dme-2* allele transmission by the *nDME<sup>CTD</sup>***  
 851 **transgene.**  
 852

Female	Male parent	F1, DME/ <i>dme-2</i>	F1, DME/ <i>dme-2</i> ; <i>nDME<sup>CTD</sup></i>	<i>nDME<sup>CTD</sup></i> transmission rate (%)	<i>p</i> for 1:1†
Col-0	<i>dme-2/dme-2</i> ; <i>nDME<sup>CTD</sup></i> /~ Line 1	32	62	66	2.0E-3
Col-0	<i>dme-2/dme-2</i> ; <i>nDME<sup>CTD</sup></i> /~ Line 2	3	50	94.3	1.1E-10
Col-0	<i>dme-2/dme-2</i> ; <i>nDME<sup>CTD</sup></i> /~ Line 3	8	34	81	6.0E-5
Col-0	<i>dme-2/dme-2</i> ; <i>nDME<sup>CTD</sup></i> /~ Line 4	9	44	83	1.5E-6

† Probability that that the deviation from the indicated segregation ration (1:1 inheritance of paternal genome with or without *nDME<sup>CTD</sup>* transgene in the F1 generation) is due to chance.

853

**a**

*dme-2/dme-2*



*dme-2/dme-2*;  
*pDME:nDME<sup>CTD</sup>/~*



*dme-2/dme-2*;  
*pDME:nDME<sup>CTD</sup>/*  
*pDME:nDME<sup>CTD</sup>*



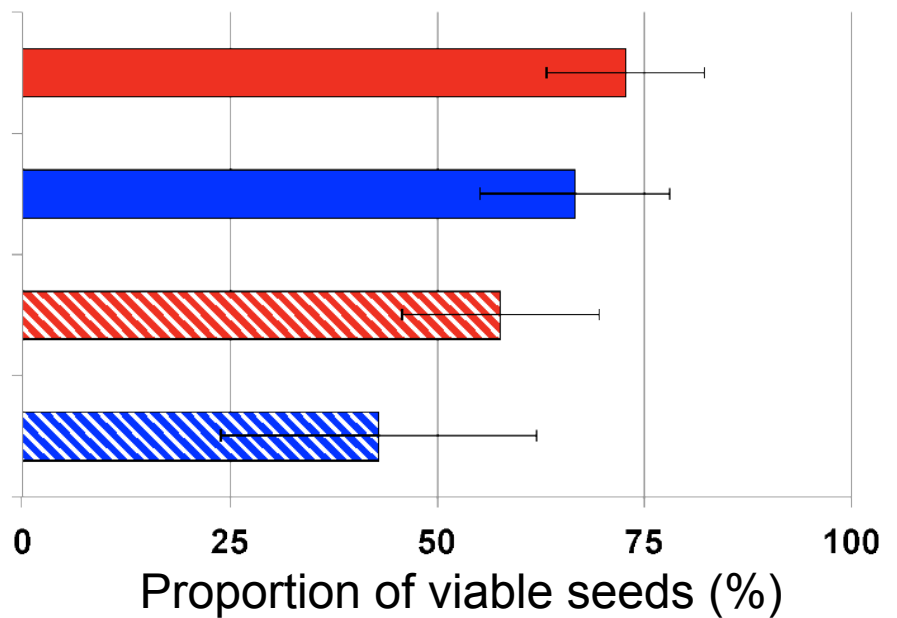
**b**

*DME/dme-2*; *nDME<sup>CTD</sup>*

*DME/dme-2*; *DME<sup>FL</sup>*

*dme-2/dme-2*; *nDME<sup>CTD</sup>*

*dme-2/dme-2*; *DME<sup>FL</sup>*



**c**

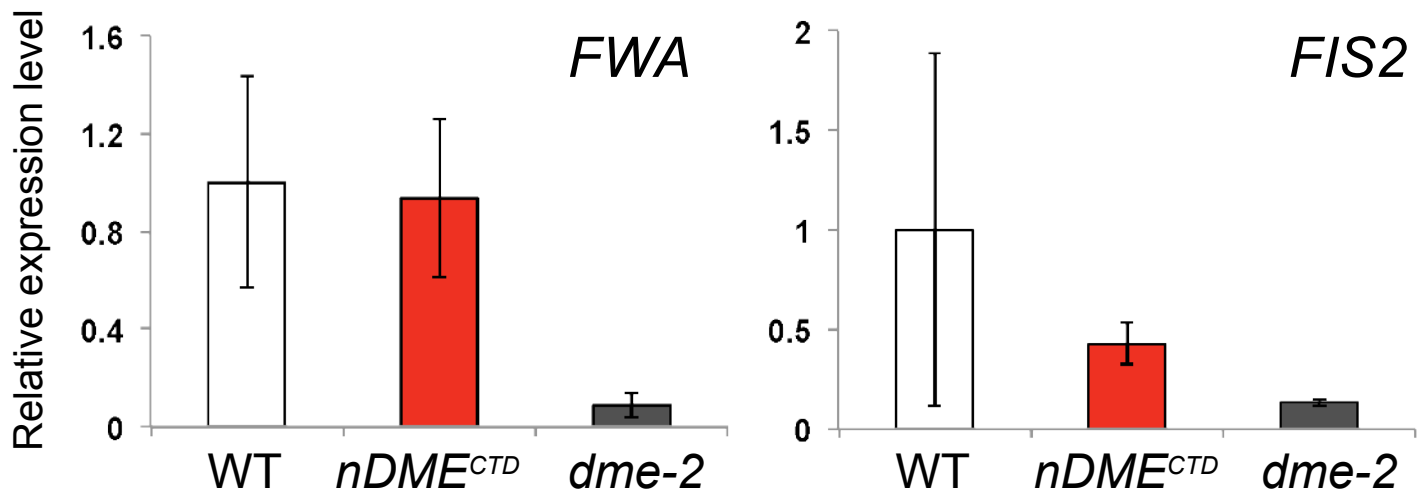
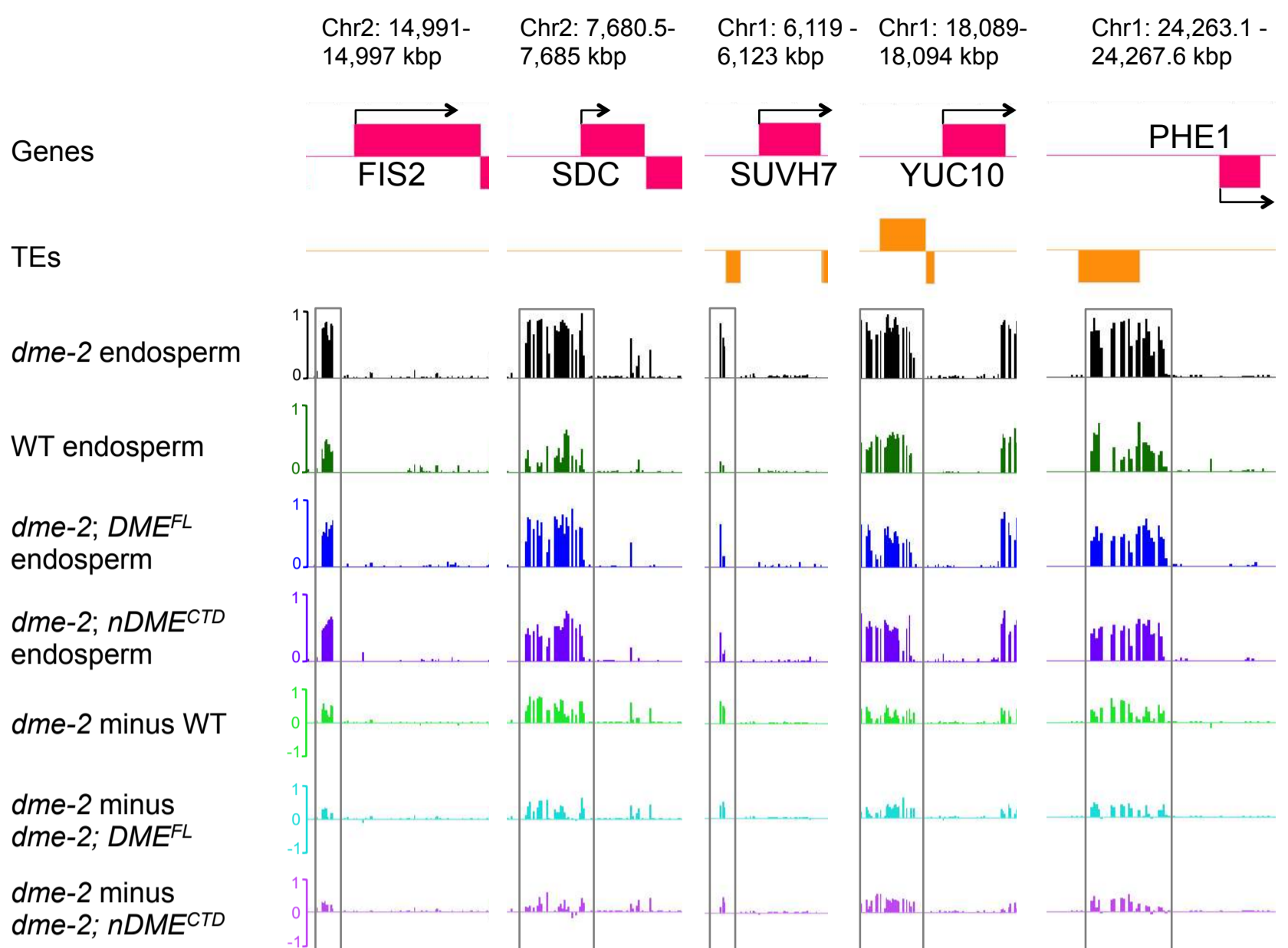
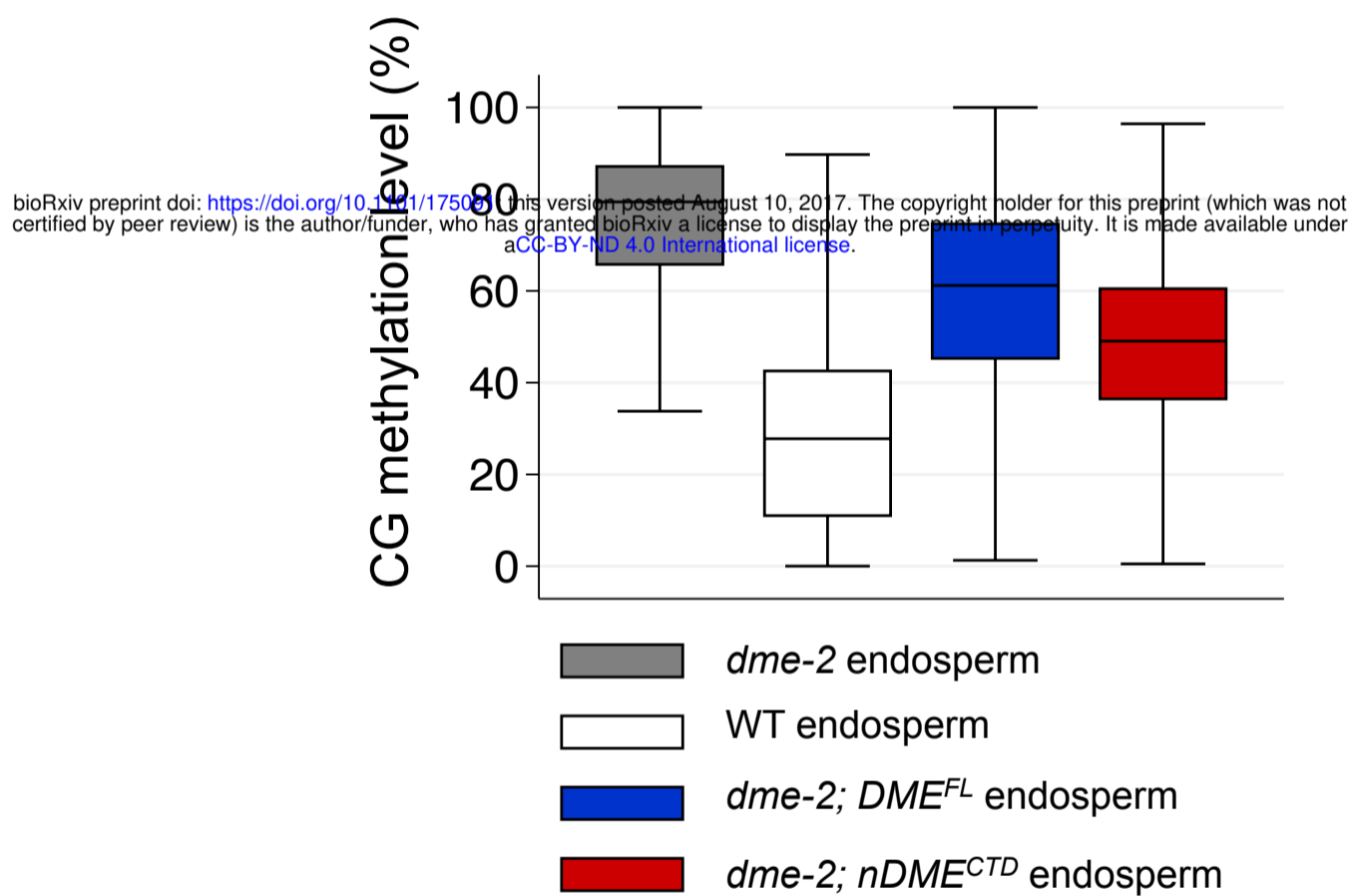


# Figure 2

**a**



**b**



**c**

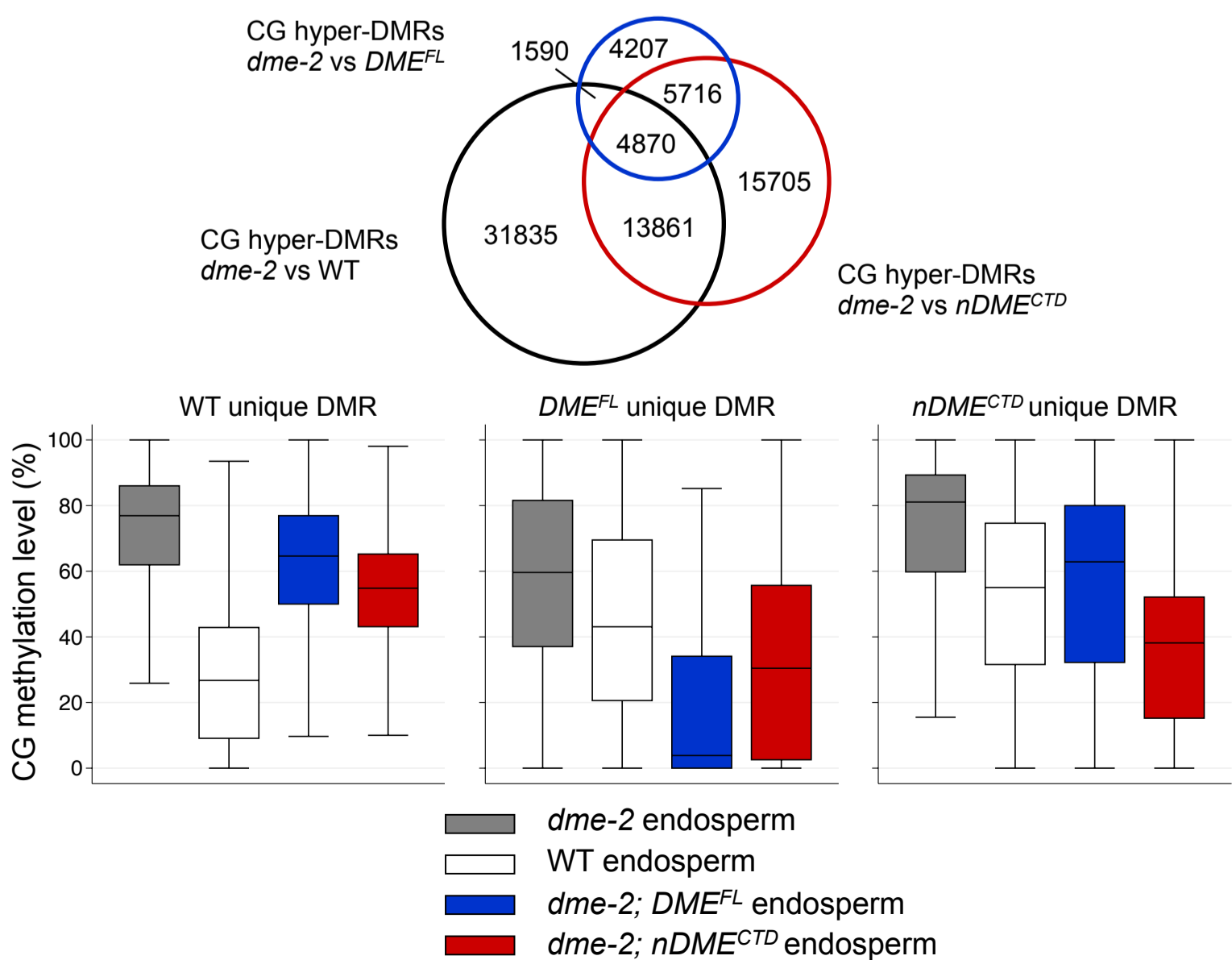
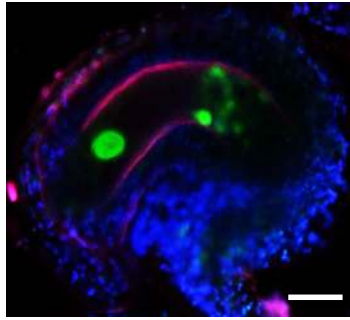




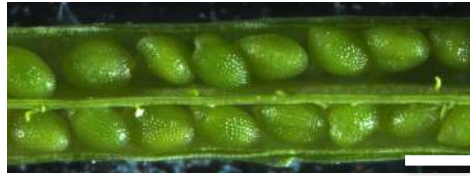
# Figure 3

**a**

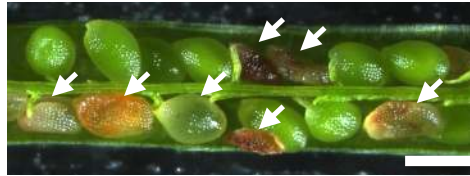


**b**

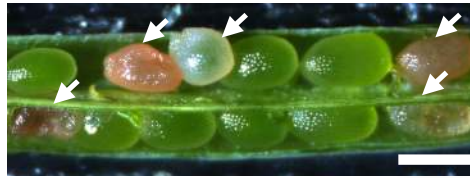
*DME/DME*



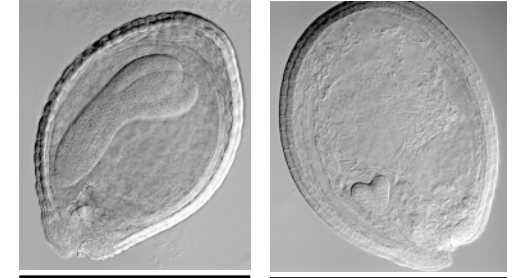
*DME/dme-2*



*DME/DME*;  
*DME<sup>NTD</sup>/~*



**c**



*DME/DME*

*dme-2/dme-2*

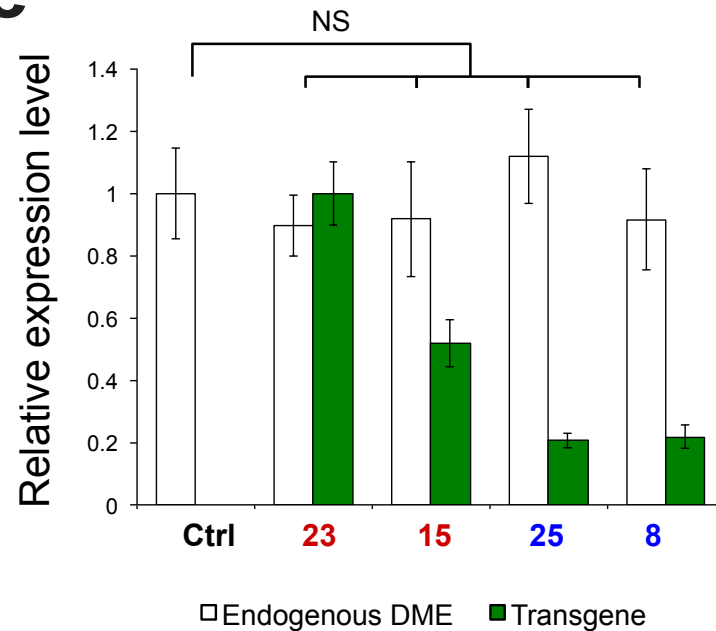


*DME/DME; DME<sup>NTD</sup>/~*

**d**

Sample	Proportion of aborted seeds (%)
Control	0
Line 23	52
Line 15	27
Line 25	0
Line 8	0

**e**



**f**

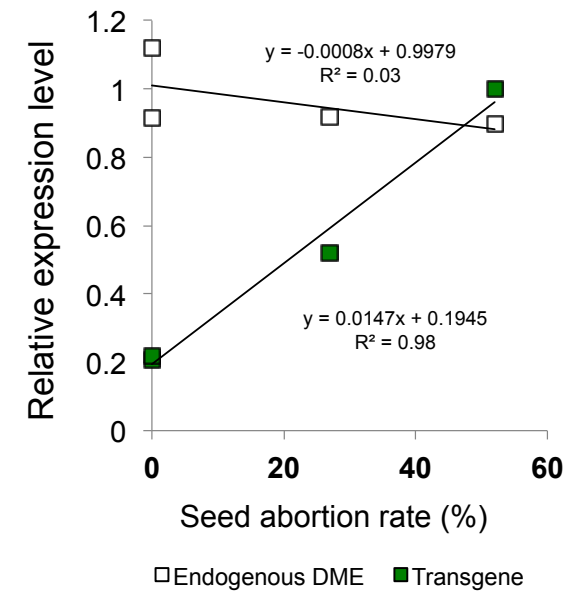
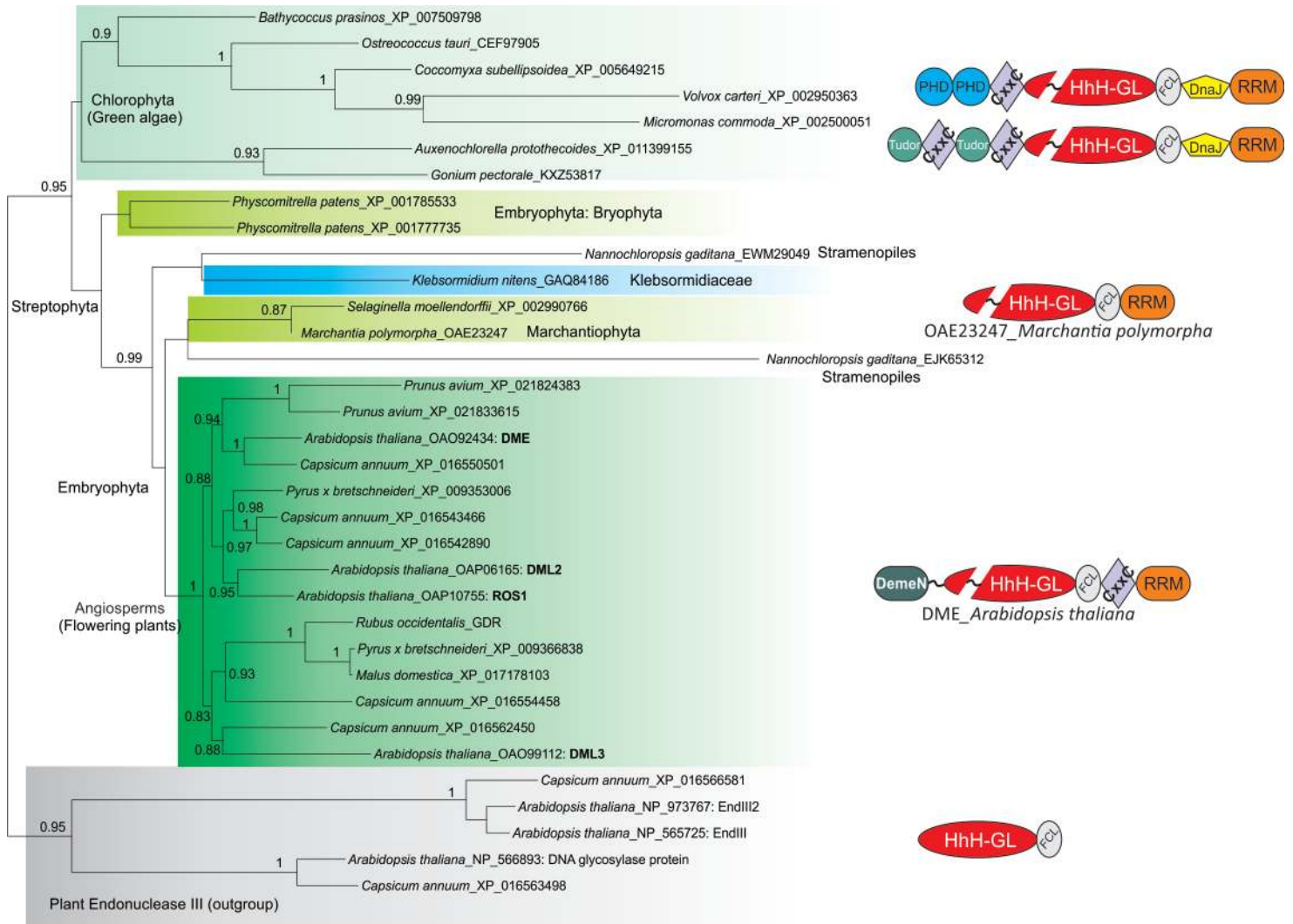
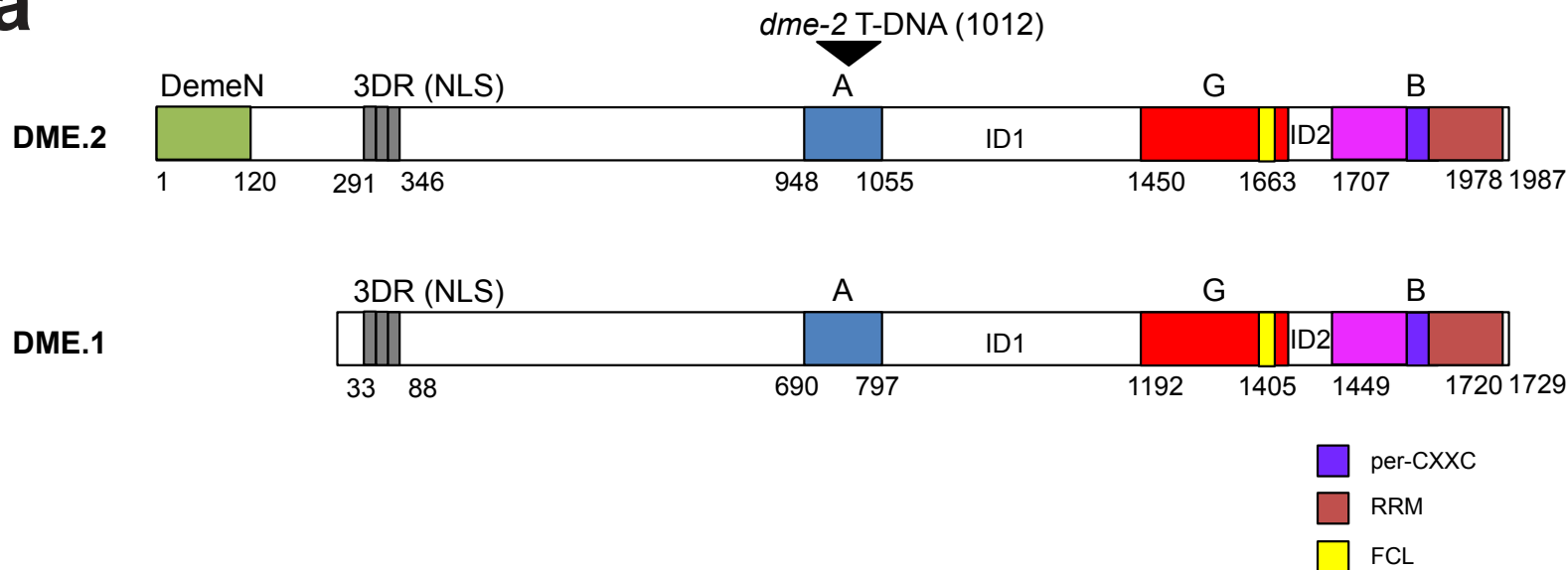


# Figure 4

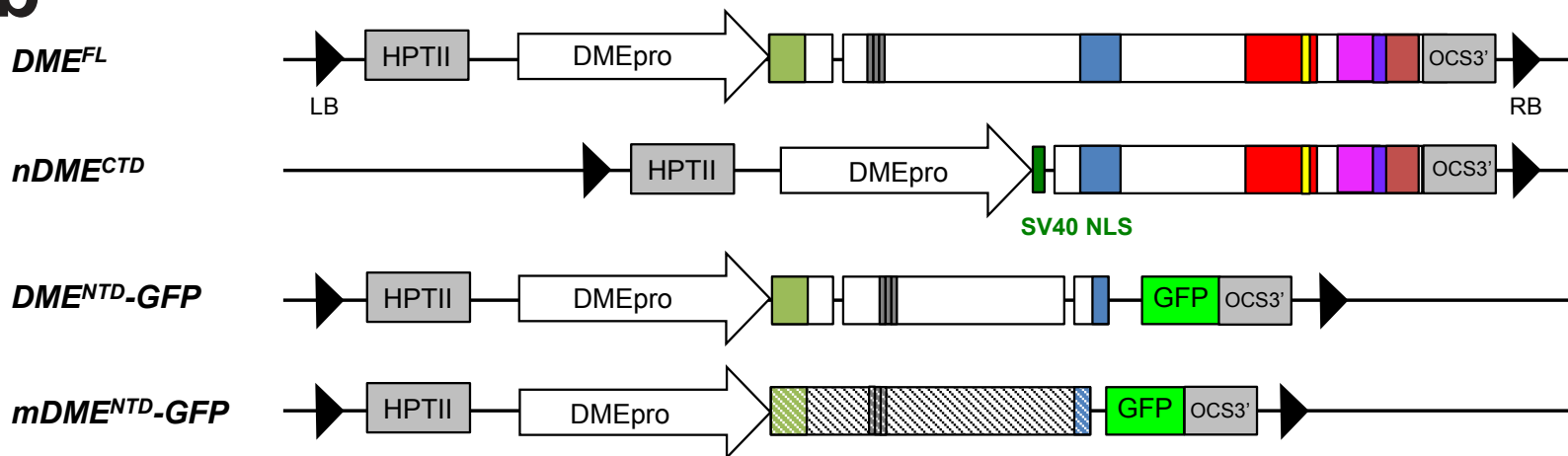


# Supplementary Figure S1

**a**

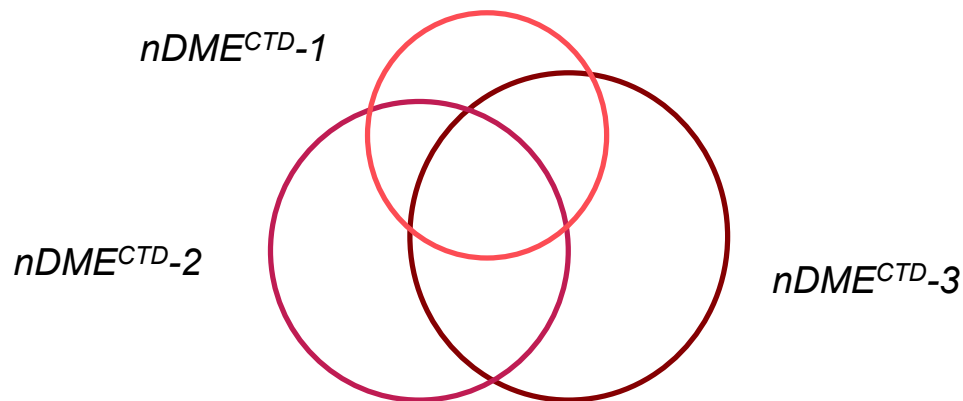


**b**

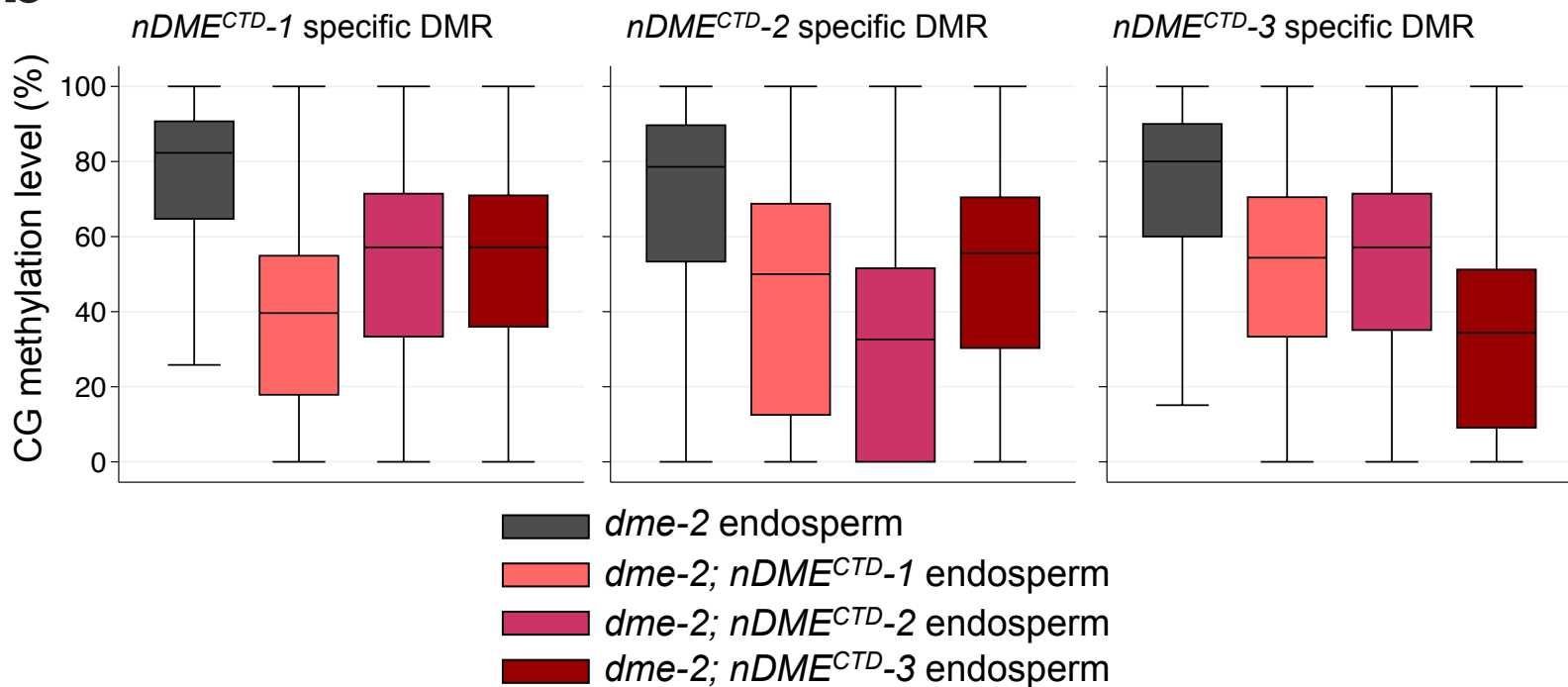


# Supplementary Figure S2

**a**

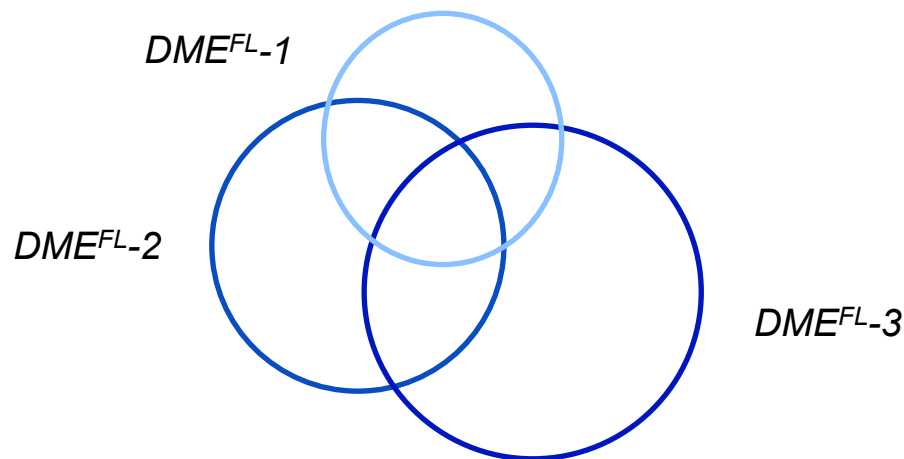


**b**

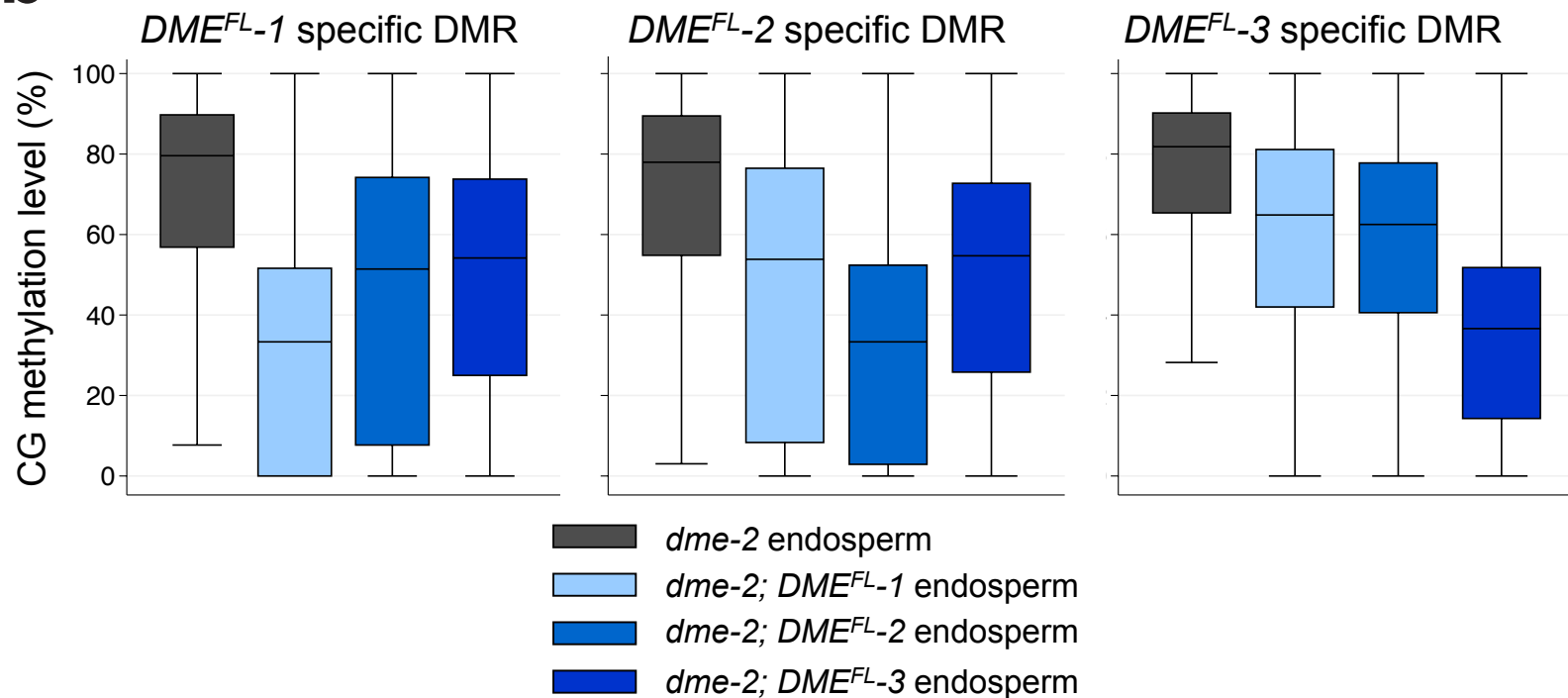


# Supplementary Figure S3

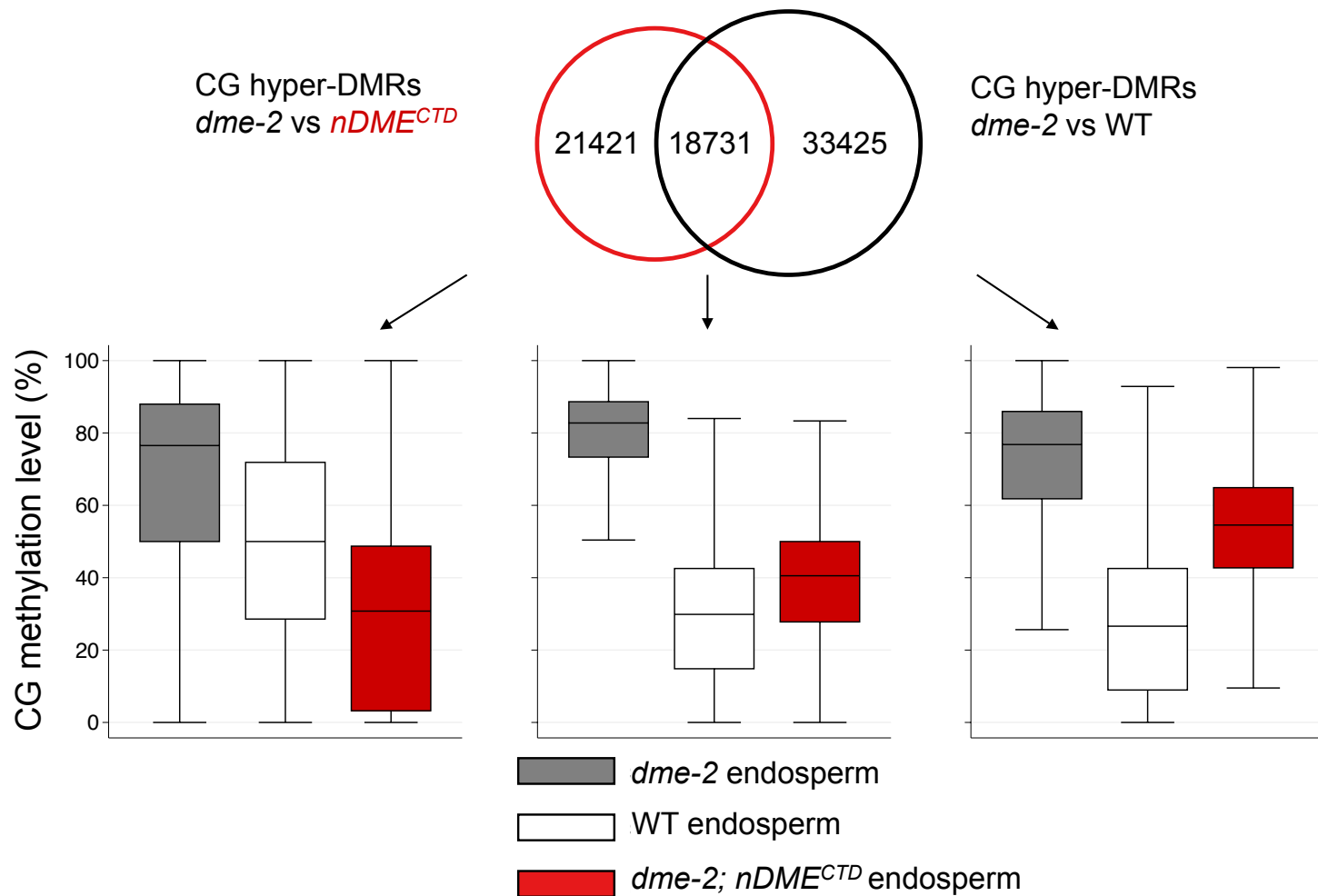
**a**



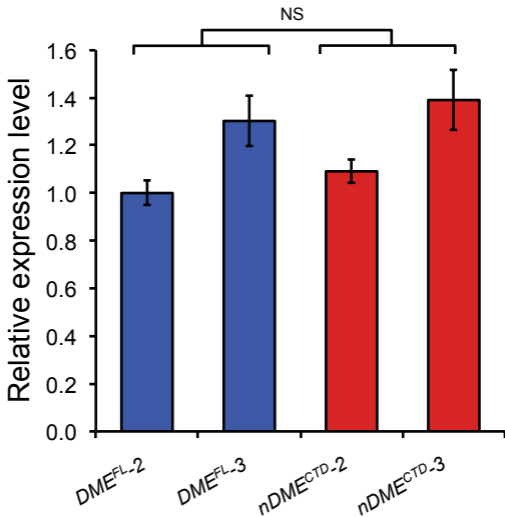
**b**



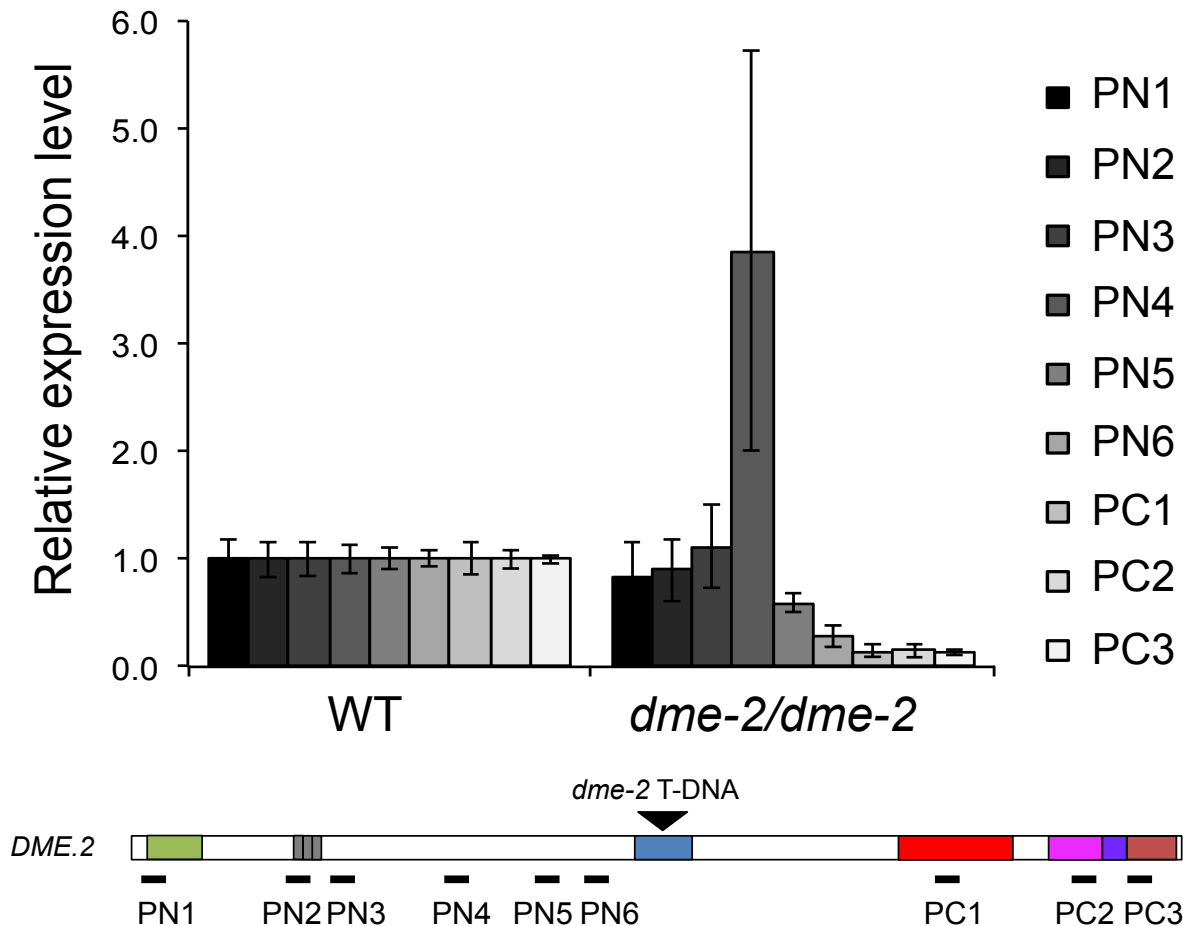
# Supplementary Figure S4



# Supplementary Figure S5

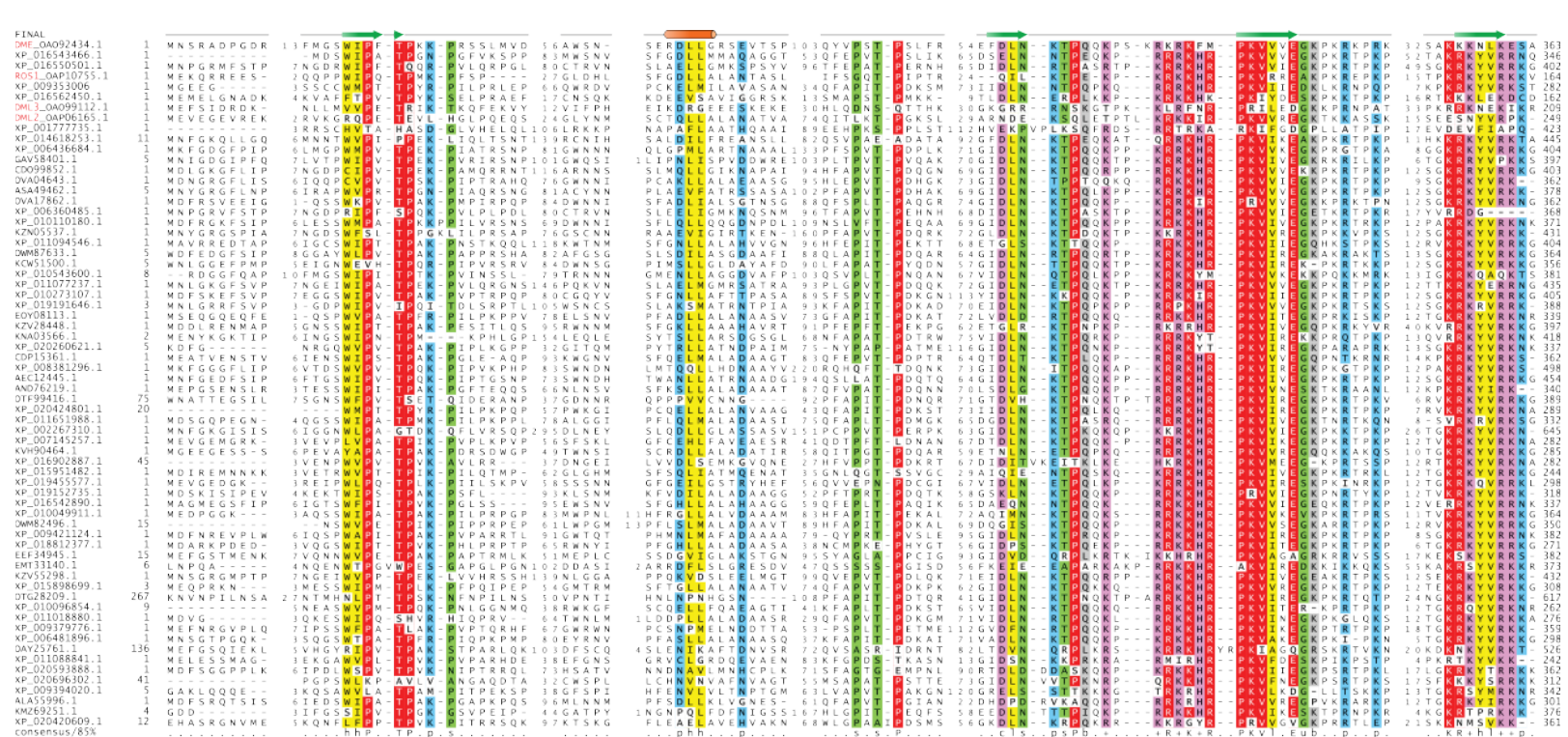


# Supplementary Figure S6





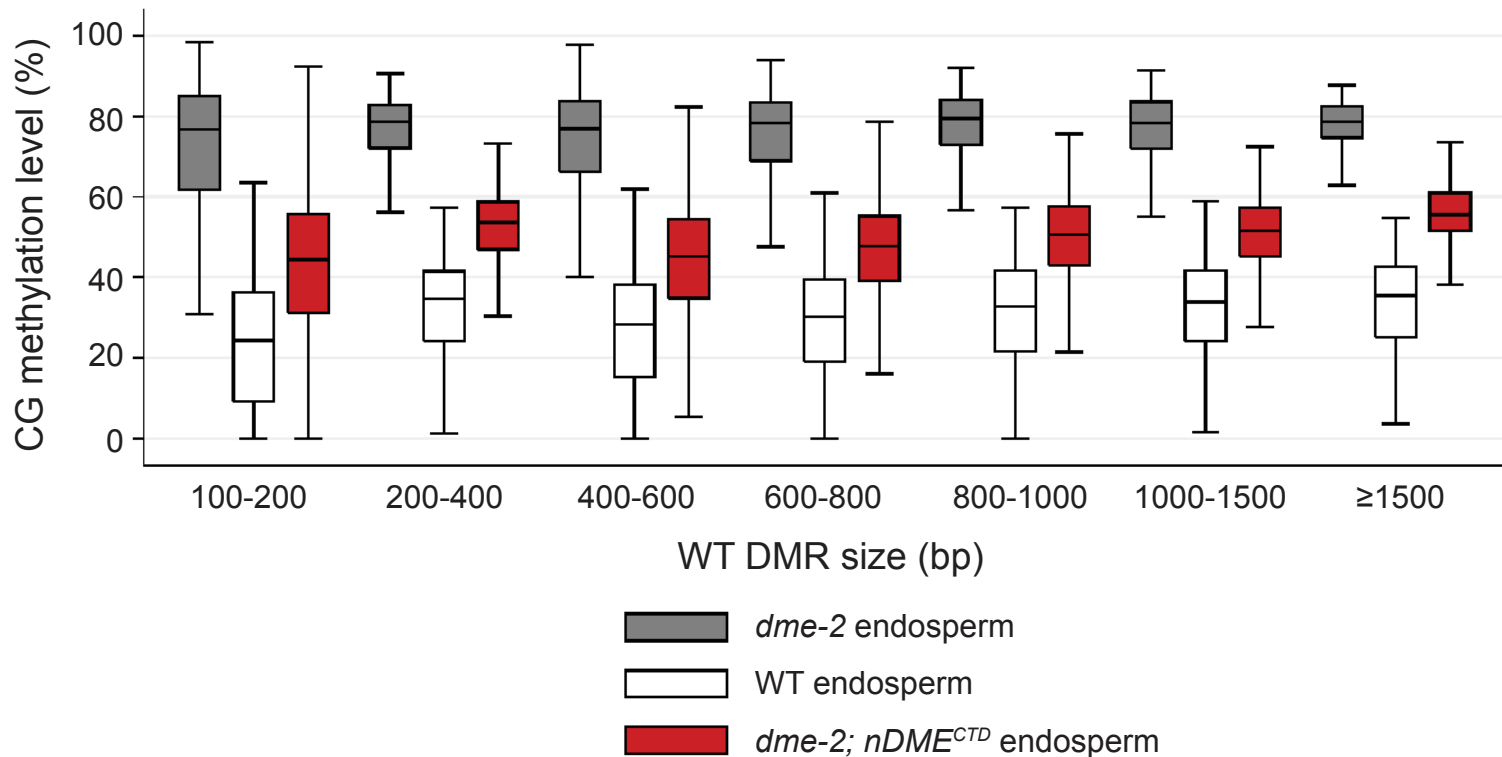
# Supplementary Figure S7



WxPxTPxK motif

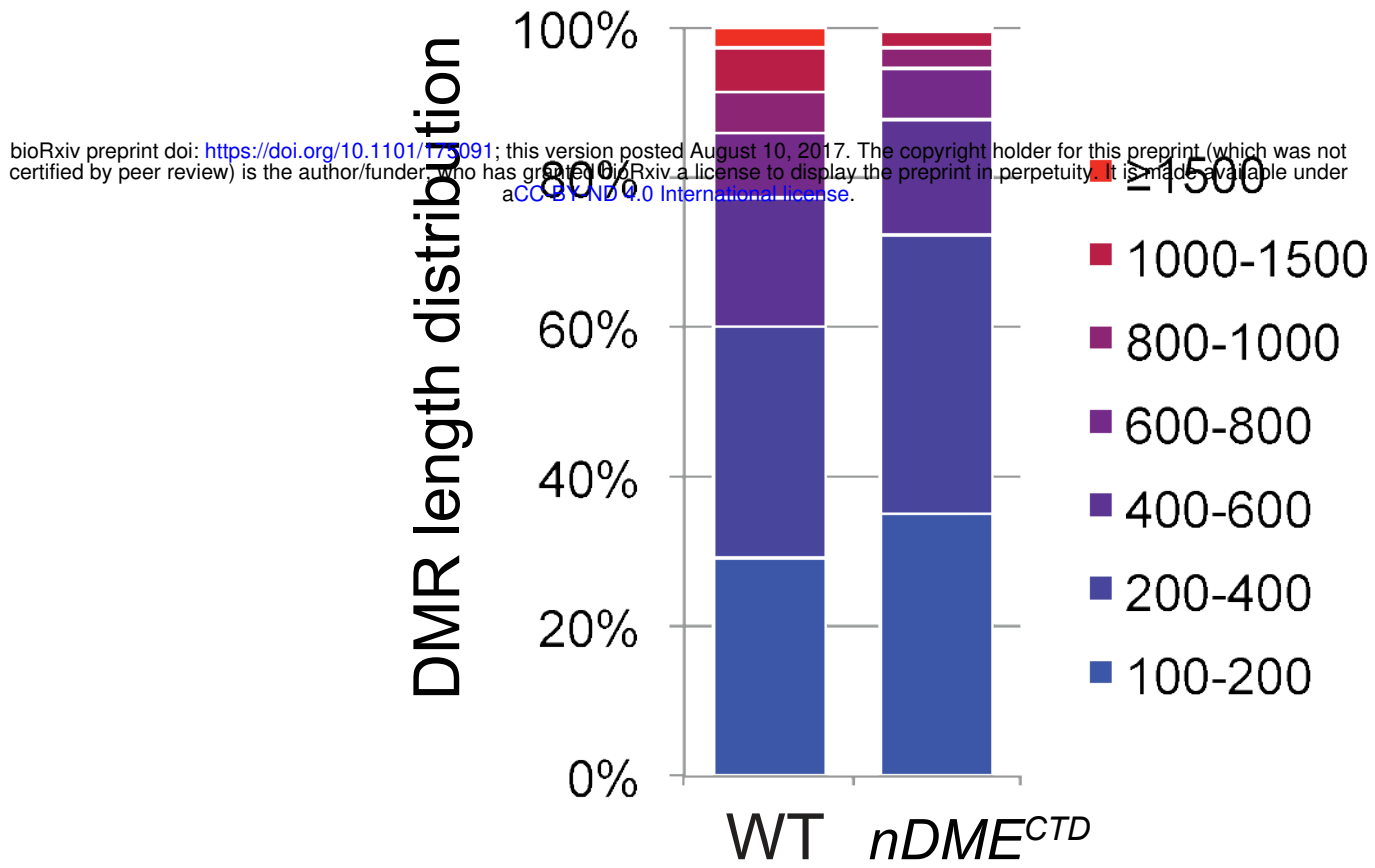
Basic amino acid rich stretch

## Supplementary Figure S8



# Supplementary Figure S9

**a**



**b**

